Quaternary Science Reviews 168 (2017) 151–181

Contents lists available at ScienceDirect

Quaternary Science Reviews

journal homepage: www.elsevier.com/locate/quascirev

An 18,000 year-long eruptive record from Volcán Chaitén, northwestern Patagonia: Paleoenvironmental and hazard-assessment implications

Brent V. Alloway [a, b, *], Nick J.G. Pearce [c], Patricio I. Moreno [d], Gustavo Villarosa [e], Ignacio Jara [f], Ricardo De Pol-Holz [g], Valeria Outes [d]

[a] School of Environment, The University of Auckland, Private Bag, 92019, Auckland, New Zealand
[b] Centre for Archaeological Science (CAS), School of Earth and Environmental Sciences, University of Wollongong, Wollongong, NSW 2522, Australia
[c] Department of Geography & Earth Sciences, Aberystwyth University, SY23 3DB Wales, United Kingdom
[d] Instituto de Ecología y Biodiversidad, Departamento de Ciencias Ecológicas, Universidad de Chile, Casilla 653, Santiago, Chile
[e] IPATEC, CONICET-Universidad Nacional del Comahue, Bariloche, Argentina
[f] School of Geography, Environment and Earth Sciences, Victoria University of Wellington, PO Box 600, Wellington, New Zealand
[g] GAIA-Antártica, Universidad de Magallanes, Avda. Bulnes 01855, Punta Arenas, Chile

ARTICLE INFO

Article history:
Received 17 January 2017
Received in revised form
25 April 2017
Accepted 12 May 2017
Available online 24 May 2017

Keywords:
Northwestern Patagonia
Tephrostratigraphy
Volcán Chaitén
Volcán Michimahuida
Cha-1

ABSTRACT

The 2008 eruption of Volcán Chaitén (VCha) in northwestern Patagonia was the first explosive rhyolitic eruption to have occurred within a century and provided an unprecedented scientific opportunity to examine all facets of the eruption ranging from magma rheology/ascent rates to ash-fall effects on biota and infrastructure. Up to very recently it was thought that the latest eruption prior to the 2008 event occurred *c.* 9750 cal. a BP. Although a number of researchers have recognised additional eruptive products, but their stratigraphy, age, and geochemical attributes have not been systematically described and/or recorded. In this study, we provide a detailed examination of andic cover-beds and tephra-bearing lake sequences located both proximally and distally to VCha, which record a series of hitherto unknown rhyolitic eruptive products and place all previous observations firmly within a coherent stratigraphic framework. Through major- and trace-element glass shard geochemistry we are able to confidently verify eruptive source. A total of 20 discrete tephra beds are recognised, with at least 10 having widespread areal distributions and/or depositional imprints broadly comparable to, or greater than, the 2008-tephra event. This record indicates that VCha has been continuously but intermittently active as far back as the end of the Last Glacial Maximum (*c.* 18,000 cal a BP) with two dominant, genetically related magma types and an intermediary 'mixed' type. Before this the eruptive record has been largely obscured and/or erased by widespread Andean piedmont glaciation. However, based on the tempo of VCha activity over the last *c.* 18,000 years, older VCha eruptives can be anticipated to occur as well as future hazardous explosive events. The new eruptive inventory will ultimately be useful for correlating equivalent-aged sequences and refining long-term eruptive tempo as well as corresponding temporal changes in magmatic evolution.

1. Introduction

The 2008 eruption of Volcán Chaitén (VCha) in southern Chile was the first explosive rhyolitic eruption to have occurred globally within the last 100 years and has provided an unprecedented scientific opportunity to examine all facets of this type of eruption ranging from magma ascent rates (Castro and Dingwell, 2009), surface deformation (Wicks et al., 2011), eruptive products (Lara, 2009; Watt et al., 2009; Alfano et al., 2011, 2016) to ash-fall modelling (Osores et al., 2013) as well as ash-fall effects on biota (i.e. Martin et al., 2009; Henríquez et al., 2015) and infrastructure. In

* Corresponding author. School of Environment, The University of Auckland, Private Bag, 92019, Auckland, New Zealand and CAS, University of Wollongong, Wollongong, NSW 2522, Australia.
E-mail address: brent.alloway@gmail.com (B.V. Alloway).

http://dx.doi.org/10.1016/j.quascirev.2017.05.011
0277-3791/

an earlier reconnaissance study by Naranjo and Stern (2004), tephra sourced from VCha was first recognised and mapped. In that study, one prominent pumiceous lapilli bed (Cha-1) was indirectly dated at <9370 ± 60 ^{14}C a BP (10,533 cal a BP) from charcoal within a closely underlying surge deposit (now identified as Lepué Tephra; Alloway et al., 2017). At that time, Cha-1 was considered to represent the products of the most recent eruption of VCha prior to the 2008 event. The northward distribution of this tephra (Cha-1) was progressively extended to the vicinities of Hornopirén and Seno Reloncaví and its age was further refined to 8849 ± 74 ^{14}C a BP (9873 ± 157 cal a BP) (Watt et al., 2011).

The recent eruption of VCha in 2008 (Lara, 2009) has served as an important driver for renewed field-investigations so that its eruptive history and potential hazards posed to adjacent and downwind communities could be better clarified (i.e. Amigo et al., 2013; Lara et al., 2013; Watt et al., 2013b). Such reconnaissance studies have inevitably led to the recognition of additional VCha eruptive products.

In this study, we provide a detailed examination of the tephra-derived andic soil dominated cover-beds and tephra-bearing lake sequences adjacent to, and extending from, VCha (Fig. 1) with the objective of placing new and previous observations firmly within a coherent tephrostratigraphic framework. In order to identify VCha-sourced tephra and distinguish these from eruptive deposits from other volcanic centres, we utilize glass shard major- and trace-element compositions using grain-discrete electron microprobe (EMP) and laser ablation inductively coupled plasma mass spectrometry (LA-ICP-MS) techniques, respectively (see Supplementary Information 1.0). Ultimately this comprehensive eruptive inventory for VCha will be useful for accurately determining longer-term eruptive tempo (beyond the Holocene) as well as corresponding temporal changes in magmatic evolution. This overall objective has a direct bearing on clarifying the hazards posed from intermittent explosive activity centred at VCha upon adjacent and downwind communities.

1.1. Tephra-derived soil-forming record

To date, the most widespread VCha-sourced tephra recognised in northern Patagonia is the *c.* 9900 cal. a BP Cha-1 deposit (Naranjo and Stern, 2004; Watt et al., 2011, 2015; Amigo et al., 2013; Fontijn et al., 2016; Alloway et al., 2017). Cha-1 exposed in several road cuts north of Chaitén was correlated by Iglesias et al. (2012) to a tephra (CT2 at 230.5–213.5 cm depth) recorded within sediments of Lago Cóndor, Argentina, and located ~125 km north-east of VCha. This tephra also chronostratigraphically matched other rhyolitic tephra units found in sediment records and surface exposures in Argentina, including the white to yellow pumice lapilli tephra unit exposed in several road cuts along the Los Alerces Parque Nacional, which has previously been attributed to Volcán Michimahuida (Naranjo and Stern, 2004; Watt et al., 2011). Cha-1 can now be reliably identified 400 km northward from VCha within sediments from Lago Villarrica and Laguna Las Ranas (Fontijn et al., 2016).

A more recently erupted Chaitén tephra was also identified by Lara et al. (2013) who produced geological and historical evidence for an explosive eruption in the 17th century (AD 1625–1658) that distributed tephra eastward and resulted in rapid fluvio-volcanic aggradation and burial of alluvial terraces by dominantly pumiceous sands within valleys directly adjacent to VCha. About the same time, a sequence of three discrete rhyolitic tephra (Cha-2, -3 and -4; oldest to youngest) were recognised (Watt et al., 2013b) from a single section (F-02) just north of Chaitén township that post-dated Cha-1 and had indistinguishable glass shard major-element chemistry confirming VCha-source.

1.2. Lago Teo record

The most detailed record of eruptive activity from VCha over the last 10,000 years was identified from a sedimentary record retrieved from a small closed lake basin (Lago Teo) located 7 km southwest of VCha (Fig. 1; Moreno et al., 2015b; Henríquez et al., 2015). This lake record reveals 302-cm of organic-rich mud with 26 discrete tephra inter-beds, including the tephra generated during the 2008 VCha eruption. Deeper core penetration at Lago Teo and retrieval of older eruptive records was thwarted by the occurrence of Lepué Tephra forming an impenetrable hard-pan at ~3.02-m (Alloway et al., 2017). Tephra inter-beds within the lake sediments typically displayed concordant horizontal millimetre-to decimetre-thick beds of well sorted coarse to fine ash with sharp upper and lower contacts. Tephra ages were determined from an age model based on a consistent array of 23 radiocarbon dates (Moreno et al., 2015b). Of the 26 tephra represented within the Lago Teo sediment core, ten inter-beds (LTT-1, LTT-2, LTT-4, LTT-5, LTT-6, LTT-12, LTT-17, LTT-22, LTT-23, LTT-25) were identified as rhyolitic in composition and were geochemically ascribed to a VCha-source based on their tight major-element clustering as determined from EMP analysis (Moreno et al., 2015b) and could be readily distinguished from rhyolitic tephra of sourced from the Michimahuida Volcanic Complex (MimVC) (Alloway et al., 2017). In this study, we augment glass shard major-element data already presented in Moreno et al. (2015b) with new glass shard trace-element data acquired by LA-ICP-MS analysis.

1.3. Issues relating to tephra nomenclature

A difficulty encountered in this study was previous designation of numeric names for VCha-sourced tephra as well as tephra inferred from, and named after, other eruptive sources. For instance, the widespread rhyolitic pumiceous lapilli with an age of <10,533 cal a BP that was termed Cha-1 by Naranjo and Stern (2004). Subsequently recognised rhyolitic tephra post-dating Cha-1 from this same sector were termed Cha-2, -3 and -4 (older to younger) by Watt et al. (2013b). The VCha-2008 tephra occurring at ground surface was then considered the fifth VCha eruptive (Cha-5) recognised. The main difficulty in dealing with these designations is how to label or accommodate additionally recognised VCha-sourced tephra (both older and younger than Cha-1) that are likely encountered through the course of subsequent stratigraphic studies and particularly, reconciling correlation of tephra from the soil-forming environment to lake sediments where more detailed tephra records are better preserved (e.g. Lowe and Alloway, 2015). This difficulty is further compounded by inferences of likely source given alongside the numerically named tephra. For instance, Mic2 named by Naranjo and Stern (2004) is now sourced from VCha (Watt et al., 2013b), and not from Volcán Michimahuida as originally thought and/or implied by its designation of name. Similarly, Cor-1 (Naranjo and Stern, 2004) is now considered erupted from MimVC (Alloway et al., 2017), and not from Volcán Corcovado.

While these designations were entirely appropriate for earlier reconnaissance work, there now needs to be some formal redefinition of their names especially since some tephra are being widely recognised and mapped in proximal through distal regions. The most efficient way of dealing with these issues is to designate formal names for *mappable* tephra layers after prominent local geographical places and/or points from areas where these layers are represented (and without numeric labelling and/or inference to eruptive source). The designation of tephra type and/or key reference sections should also be considered in accordance with the International Stratigraphic Guide (e.g. Murphy and Salvador, 1999). In this way, there are no forward difficulties or confusion arising

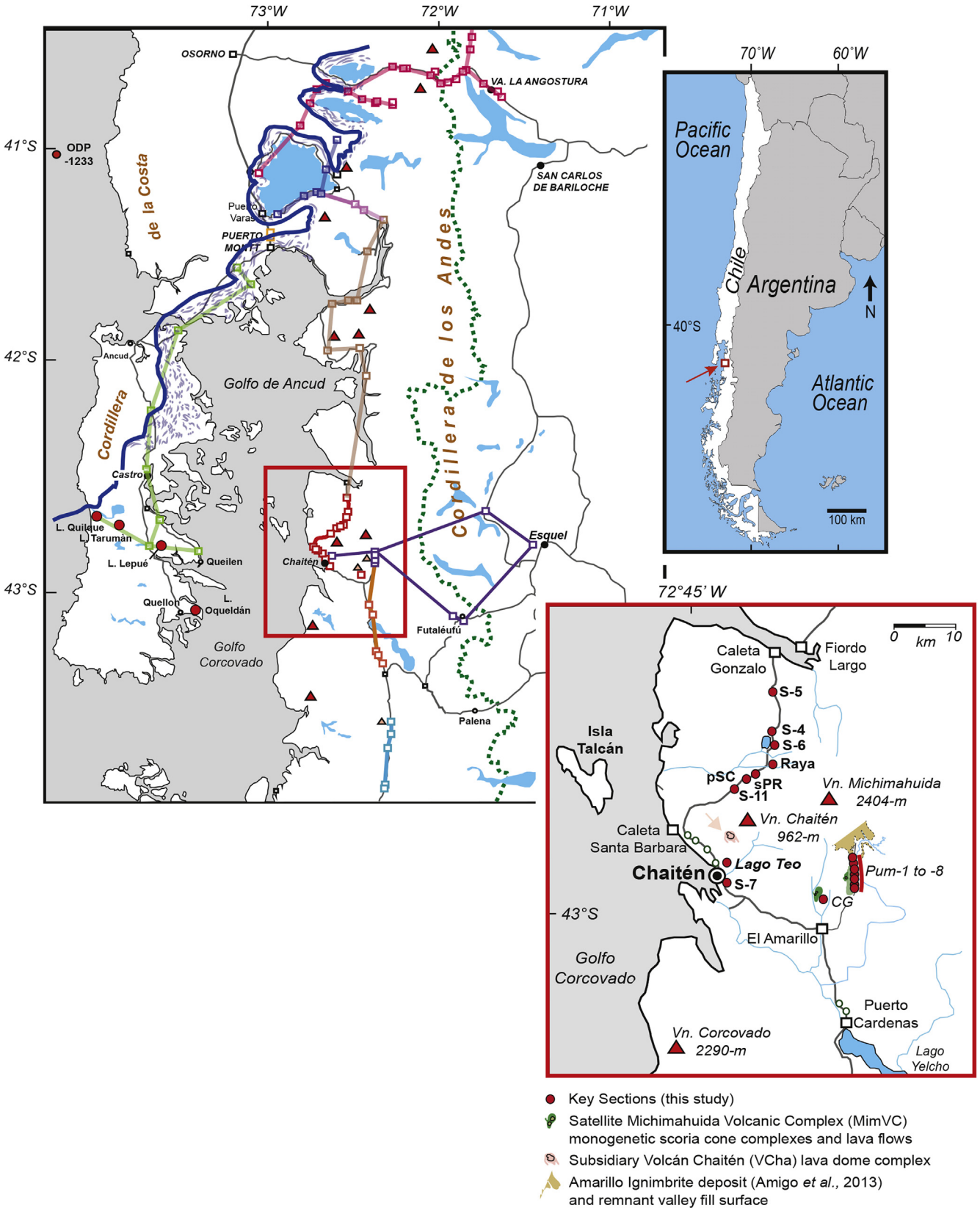

Fig. 1. Location of the study area in Chaitén Sector of northwestern Patagonia. The regional array of described tephra sections as part of this study are shown by transect lines illustrated in different colours. The maximum extent of Last Glacial Maximum (LGM) ice lobes within this region (modified from Plates 1–4 *in* Denton et al., 1999 and Moreno et al., 2015a) are indicated in blue. Indicated within the map inset are the locations of key cored lakes situated on Isla Grande de Chiloé (Lago Quilque, Lago Tarumán and Lago Lepué), Lago Teo located close to Chaitén township, key descriptive sections (this study), satellite Michimahuida Volcanic Centre (MimVC) monogenetic scoria cone complexes and lava flows, newly recognised subsidiary VCha lava dome complex, and Amarillo Ignimbrite deposit and its remnant valley fill surface (Amigo et al., 2013; Alloway et al., 2017). (For interpretation of the references to colour in this figure legend, the reader is referred to the web version of this article.)

from accommodating newly recognised tephra within an established stratigraphic framework involving multiple tephra sourced from the same and/or different eruptive centres. To this end, it is our intention to drop the numeric designations and ascribe a scheme of geographic place-names to mappable VCha-sourced tephra as well as designate key sections for future reference (see Supplementary Information 2.0).

1.4. Andic soil cover-beds

In this study, it is necessary to adopt a 'pedo-volcanological' approach in characterising dominantly volcanic-derived stratified soil cover-bed deposits affected by intense post-depositional weathering and disturbance in the wet, hyper-humid volcanic environments of northwestern Patagonia. Not only does the intensity of pedogenic weathering in this region effectively mask fine-grained and/or thin tephra inter-beds within soil-dominated cover-beds, it potentially compromises the morphological expression of the tephra as well as its constituent geochemistry and grain-size characteristics – all attributes of which are fundamental in tephra correlation. Within the Chaitén sector, cover-bed sections typically comprise predominantly tephra-derived, fine-textured soil materials separating thick and/or coarse-grained lithologically distinct tephra beds and volcaniclastic detritus that have resisted post-depositional weathering and pedogenic mixing. Intervening soil materials are characterised by distinct 'andic' properties of high 1500 kPa (15-bar) water retention, high porosity and low bulk density, and are dominated by nanocrystalline materials chiefly allophane, ferrihydrite and metal-humus complexes (Parfitt and Clayden, 1991; McDaniel et al., 2012; Soil Survey Staff, 2014). Each andic inter-bed forms part of a soil accession and represents a period of intermittent accretion of fine-grained detritus (dominantly tephra) with subsequent rapid weathering (Alloway et al., 1995) - a process known as '*up-building pedogenesis*' (see Lowe and Tonkin, 2010). Under these conditions, an andic soil inter-bed does not need to be genetically related to the eruptive phase that generated either the underlying, or overlying, tephra bed. In describing the material that comprises these andic soil inter-beds, soil particle size class names have not been used. The concept of either texture or particle size is here considered not applicable to materials dominated by nanominerals, particularly as they typically cannot be dispersed readily (e.g. Alloway et al., 1992a). Instead selected classes (i.e. pumiceous, ashy, medial, hydrous) from the Keys to '*Soil Taxonomy*' (Soil Survey Staff, 2014) are adopted to describe the field characteristics of the andic soil material. These classes based on combinations of both particle size and mineralogy, were originally proposed by Smith (1984) as improved criteria for classifying volcanic soils (Andisols).

1.5. Tephra isopachs

In this study, isopachs are deliberately not drawn nor are provisional volumes calculated – stratigraphic observations at the present time are simply too sparse though some first-order indication of magnitude can be assessed from primary tephra thicknesses within small lakes located distally from source. While isopach maps may serve to provide a preliminary indication of downwind distributions from an inferred eruptive source, some are clearly wrong (for instance, Mic2 was later correlated with Cha-2 by Watt et al., 2013b; Cor-1 was correlated with Lepué Tephra sourced from Volcán Michimahuida by Alloway et al., 2017). Tephra measurements are not assisted by the sparseness of access and observation points extending across the Andes, and usually road sections that typically traverse moderate to very steep-sloped mountain fronts. Here, secondary remobilisation and over-thickening affecting thickness and grain-size parameters are common occurrences within this high rainfall region (~2400-mm per yr). Fine-grained and/or thin tephra layers within the soil-forming realm are laterally discontinuous and rarely have definable (sharp) lower and upper contacts but instead are usually dispersed within the soil matrix making thickness measurements additionally difficult to acquire. At this stage, the utility of such isopach maps, while broadly indicative, is limited especially given the spatial spread of observation points and/or discriminating geochemical attributes that may assist in correct correlation of a distal tephra to its source-proximal equivalent. Thicknesses attained from small-sized lakes and/or bogs are considered in this study to be the most optimal, although tephra preservation might still be influenced by sediment focusing and compaction.

2. Stratigraphy and age

2.1. Upper set of VCha-sourced tephra (<850 cal a BP)

In proximal upwind (west) and distal downwind (east) regions extending from VCha, primary and secondary remobilised ash products from the VCha-2008 eruption are observed frequently mantling the present-day ground surface. Shortly after the commencement of eruptive activity, ash was mapped by Watt et al. (2009) and Alfano et al. (2011, 2016), with the former study calculating ~1.6×10^{11} kg of ash (dense rock equivalent volume of 0.07 km^3) deposited eastwards over ~2×10^5 km^2 of Argentina within the first week of the eruption. Several discrete ash-fall units with bimodal size distribution were discerned and were related to more energetic eruptive phases and ash-cloud aggregation processes. The overall compositional homogeneity of the VCha-2008 ash also suggested a highly evolved magma at ~5 ± 0.5-km depth that rapidly ascended before explosive fragmentation (Castro and Dingwell, 2009) and without the compositional complexities associated with mafic magma replenishment occurring at depth within the sub-volcanic system.

Tephrostratigraphy from soil cover-bed sections northwest and southeast of VCha is shown in Figs. 1 and 2. Informal field designations for tephra beds are section-specific and indicated alongside corresponding stratigraphic columns (i.e. for Pumalín-2 Section in Fig. 2: Pum-2-1, Pum-2-2 etc.). Radiocarbon sample position and acquired ages (expressed as ^{14}C *a BP*) are indicated beside stratigraphic columns as well as being listed in Table 1.

At most sections, two closely spaced rhyolitic tephra layers can be identified below the ubiquitous VCha-2008 tephra occurring on the present-day ground surface. In source-proximal sections located in the north-east sector these tephra are typically associated with weakly developed paleosols (medial-ashy) and/or organic-rich muds formed between primary block-and-ash flow and/or secondary remobilised breccia deposits of predominantly banded rhyolite (Section 11, 11-7 and 11-6) and fluvio-volcanic gravels and sands (Puente Salvador Coma, pSC-4/5 and 2/3) (Fig. 3). At these localities, bedding architecture indicate both co-eruptive fall and pyroclastic density current (PDC) emplacement. The upper and lower tephra are here formally named Grande and Vilcún Tephras, respectively. In more distal sections occurring in the south-eastern (downwind) sector (i.e. Pumalín-2) Grande and Vilcún Tephras occur as centimetre-thick, massive to normal graded, coarse to fine vitric ash within weakly developed (ashy-medial) paleosols and are separated by scoriaceous (P2-T4) and pumiceous (P2-T5) tephra from adjacent centres within the MimVC. Correlation is affirmed from a combination of associated stratigraphy, radiocarbon chronology (see Fig. 2) and glass shard chemistry (see Section 4.0).

At Lago Teo, five discrete VCha-sourced tephra beds (LTT-1, -2,

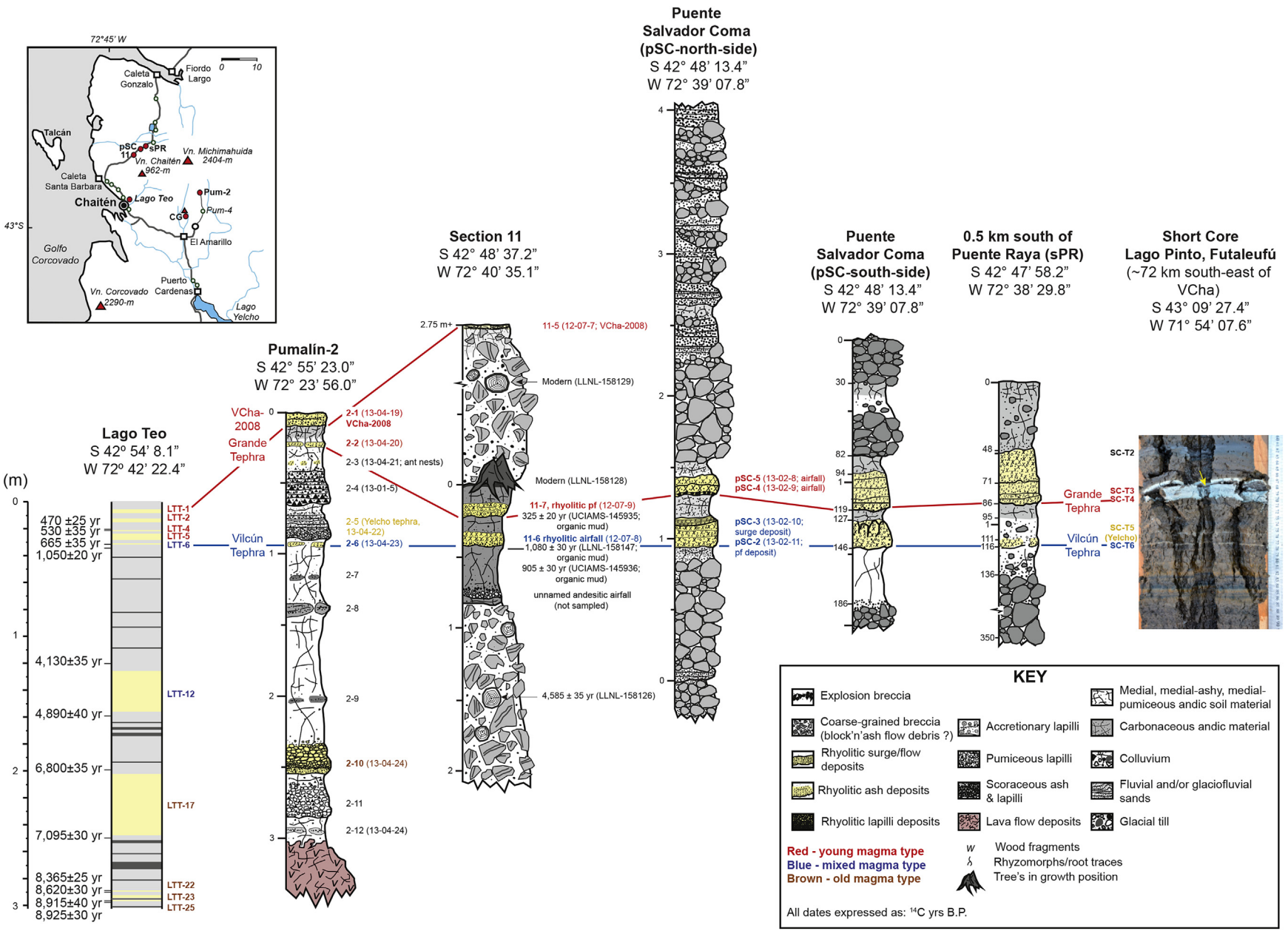

Fig. 2. Stratigraphic columns showing the correlation of the upper set of Volcán Chaitén (VCha)-sourced tephra (<850 cal a BP) with enveloping sediments and volcaniclastic deposits from Lago Teo (Moreno et al., 2015b), Pumalin-2 in the south-east sector, Sections 11, Puente Salvador Coma (pSC), Puente Raya immediately northward of VCha, and Lago Pinto located ~72 km south east of VCha in the vicinity of Futaleufú. Red and blue line designations indicate VCha-sourced tephra of young and mixed magma type, respectively. Colour-coded numeric designations for tephra section descriptions (and sample numbers) along with the position of radiocarbon dates (presented as ^{14}C yrs BP) are also indicated. (For interpretation of the references to colour in this figure legend, the reader is referred to the web version of this article.)

Table 1
Radiocarbon samples and ages associated with VCha-sourced tephra.

Location	Laboratory Code	Sample type	Sample position	^{14}C AMS age (^{14}C yr a BP)	Calibrated Age‡ (± 1σ) (cal. a BP)	95 % HPDF* (cal. a BP)
Section 11 (see Fig. 2)	LLNL-158129	Wood (outermost trunk)	Oriented small tree encapsulated within upper breccia deposit	Modern		
	LLNL-158129	Wood (outermost trunk)	Truncated tree in position of growth at basal contact of upper breccia deposit	Modern		
	UCIAMS-145935	Organic mud	Immediately beneath 11-7 (PDC of VCha-source)	325 ± 20	375 ± 48	444-365
	UCIAMS-145936	Organic mud	Immediately beneath 11-6 (airfall of VCha-source)	905 ± 30	769 ± 40	806-718
	LLNL-158147	Organic mud	Immediately beneath 11-6 (airfall of VCha-source)	1080 ± 30	943 ± 34	984-905
	LLNL-158126	Wood (outermost trunk)	Oriented small tree encapsulated within lower breccia deposit	4585 ± 35	5182 ± 90	5319-5046
Alerce-6 (see Fig. 4)	UCIAMS-145500	Charcoal	Dispersed in andic medial material immediately beneath A6-1 (VCha-sourced)	4720 ± 25	5408 ± 63	5474-5316
	UCIAMS-145501	Charcoal	Dispersed in andic medial material immediately above A6-2 (Cor-2 correlative)	6190 ± 25	7058 ± 64	7160-6950
Paso Lago Blanco (S4) (see Fig. 8)	UCIAMS-145938	Charcoal	Occurring within upper surge subunit of Lepué Tephra beneath Cha-1 (*sensu stricto*, Naranjo and Stern, 2004)	9960 ± 330	11,495 ± 517	12,552-10,561
Sta. Lucía-2 (see Fig. 8)	UCIAMS-145498	Organic mud	Directly beneath Sta.L2-T2 at ~3.09 m depth below surface (VCha-sourced)	12,250 ± 45	14,103 ± 85	14,275-13,941
La Zeta, ARG. (see Fig. 8)	LLNL-158298	Organic mud	Directly above LAZ-T13 (Chana Tephra correlative)	7660 ± 30	8417 ± 32	8479-8364
	LLNL-158297	Organic mud	Directly underlying LAZ-T1 (rhyolite of unknown source)	12,935 ± 50	15,403 ± 116	15,632-15,186
	LLNL-158296	Organic mud	~0.22 cm below LAZ-T1 (rhyolite of unknown source)	13,000 ± 45	15,489 ± 116	15,715-15,275
	UCIAMS-145923	Organic mud	Immediately below JT5 (basaltic andesite of MimVC source?) at ~0.39 cm above section base	14,410 ± 60	17,507 ± 111	17,724-17,259
	UCIAMS-145922	Organic mud	Intervening between JT4 (andesite of MimVC-source?) and JT3 (VCha-sourced) at ~0.25 cm above section base	14,590 ± 60	17,729 ± 103	17,932-17,532
	UCIAMS-145921	Organic mud	Directly underlying JT3 (VCha-sourced) ~0.20 cm above section base	14,760 ± 60	17,907 ± 99	18,097-17,698
	UCIAMS-145920	Organic mud	Directly overlying glacial diamict (till) at section base	14,840 ± 70	18,005 ± 107	18,236-17,796
Puelche (see Fig. 14)	LLNL-122955	Organic mud	Directly beneath Cha-1 correlative	8720 ± 25	9619 ± 47	9699-9545
	LLNL-123029	Organic mud	Directly beneath Lepué Tephra	9,570 ± 30	10,887 ± 125	10,879-10,695
	LLNL-122953	Organic mud	Directly overlying colluvium resting on glacial diamict at section base	14,070 ± 35	17,039 ± 105	17,244-16,794
Ralún (see Fig. 14)	LLNL-122691	Charcoal	Directly beneath Cha-1 correlative	8625 ± 25	9543 ± 23	9599-9494
	UCIAMS-145484	Charcoal	~0.74 cm below base of Cha-1 correlative (between Ra-4 & Ra-5)	8,970 ± 30	10,053 ± 86	10,098-9915

Notes: ‡ The Southern Hemisphere terrestrial calibration curve (SHCal13) and OxCal Program (v. 4.2.4) were used for all samples; * Highest Probability Density Function; UCIAMS - University of California at Irving - AMS Facility; LLNL – Lawrence Livermore National Laboratory. Red, blue and brown colours indicate 'Young', 'Mixed' and 'Old' VCha magma types, Purple colour highlights Lepué Tephra from MimVC (see also Alloway et al., 2017) and green indicates tephra from yet-to-be-determined eruptive sources.

-4, -5 and -6) were recognised within the last *c.* 850 cal. a BP (Moreno et al., 2015b, Fig. 2). In the vicinity of Futaleufú (~72 km south-east of VCha), six discrete tephra-beds can be also identified over a similar time interval within the top meter of a sediment core retrieved from Lago Pinto (S 43° 09′ 27.4"; W 71° 54' 07.6"; 524-m) of which four (SC-T1, -3, -4 and -6) are rhyolitic in composition and can be ascribed to a VCha-source based on glass shard major-element chemistry. A 3-mm interval of organic mud separates SC-T3 and -T4 suggesting two very closely spaced (but nevertheless separate) eruptive events that may not be recognised as separate events within equivalent-aged correlatives occurring within the soil-forming environment (e.g. 11-7 and pSC-4/5) although multiple bedding is noted and could conceivably represent closely spaced successive deposition but without intervening soil formation and/or erosion affecting the up-building ground surface.

Exposed prominently in sections along road W-887 (e.g. Pumalín-2, Fig. 4), a brown cm-thick medium to coarse pumiceous lapilli bed (Pum-2-T5, here informally named Yelcho tephra) can be observed to intervene between a scoriaceous basaltic lapilli (Pum-2-T4) and Vilcún Tephra (Pum-2-T6), below (see Fig. 5B and lower

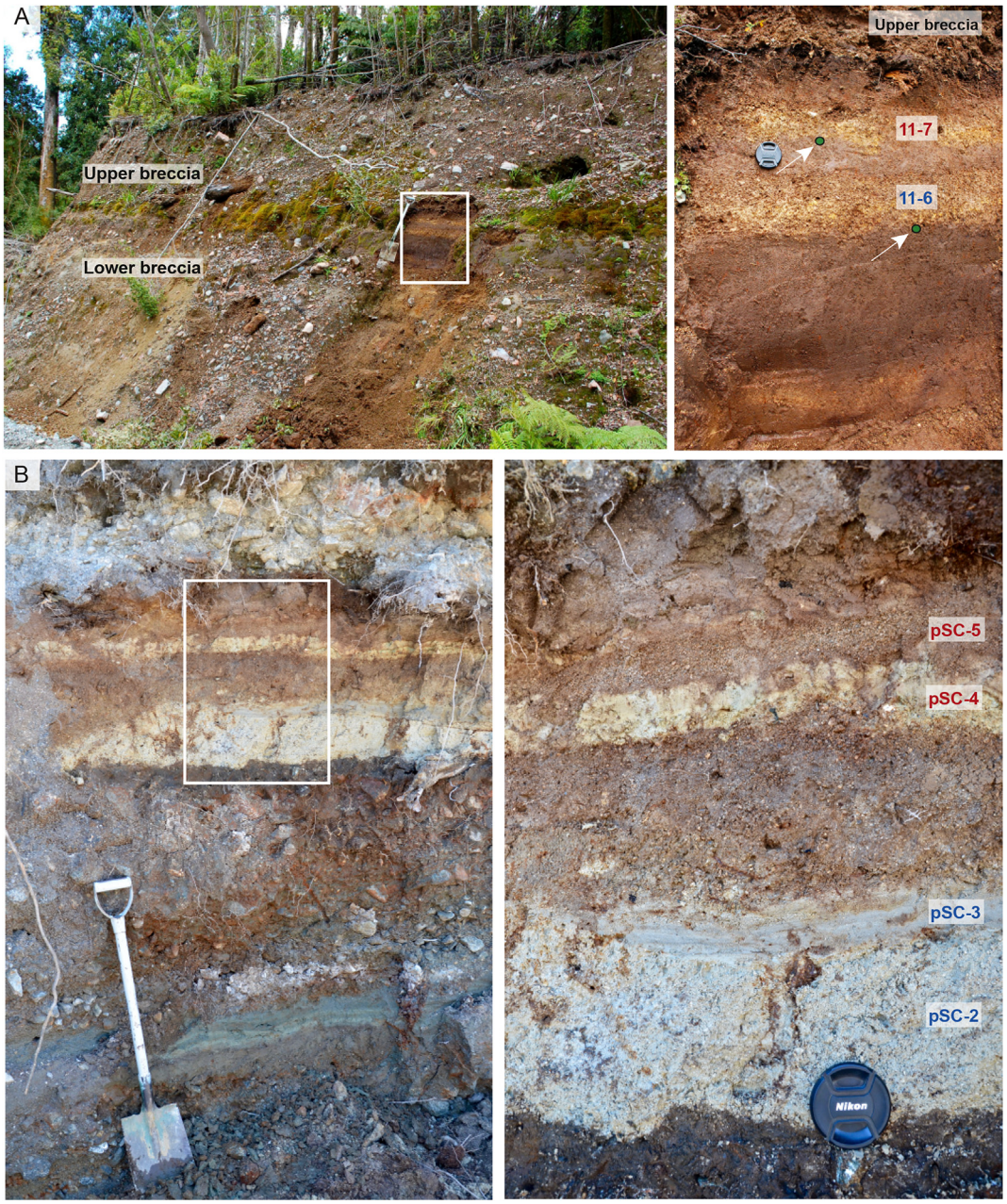

Fig. 3. The stratigraphies exposed at **(A)** Section 11 and **(B)** Puente Salvador Coma (pSC) north-side. **Inset A** indicates an interval of carbonaceous mud with interbedded tephra intervening between two metre-thick coarse-grained breccia deposits. The positions of radiocarbon samples are indicated. The two breccia deposits comprise dominantly angular, banded-rhyolite clasts containing oriented logs and vegetative material. Truncated large trees in position of growth can be observed at the basal contact of the upper breccia deposit and attests to very rapid inundation of the pre-existing forest. No charring of vegetation was discerned and it is therefore likely that these deposits are the products of older eruptive materials remobilised *en masse* by a slope failure event. Whether these events were activated by younger episodes of eruptive activity is not known. **Inset B** shows the closely-spaced tephra couplet separated by a weakly developed medial-ashy soil. The lower tephra (pSC-2/3) comprises a massive centimetre-thick pyroclastic flow directly overlain by a thinner surge unit. While, the upper tephra (pSC-4/5) comprise two centimetre-thick fall beds in direct contact and without any obvious hiatus between. Brecciated obsidian fragments occur at the base of pSC-4.

inset). The overlying basaltic lapilli bed can be traced to a satellite monogenetic cone complex situated adjacent to the Michimahuida massif and alongside the Campo Grande campsite within Parque Pumalín (Fig. 5A; Alloway et al., 2017). The construction of this cone complex diverted down-valley glacio-fluvial drainage from glaciers on the southeastern flanks of Volcán Michimahuida. The eruptive source of the intervening Yelcho tephra was, until recently, unknown. However, its correlation to a newly recognised satellite lava dome adjacent to VCha is proposed here on the basis of the glass chemistry of its pumiceous constituents in combination with its field characteristics (see Discussion Section 5.3). Vilcún Tephra, based on glass shard chemistry (see Geochemistry Section 4.0), has an unequivocal VCha-source.

2.2. Middle set of VCha-sourced tephra (pre-850 and post-11,000 cal a BP)

The middle sequence of VCha-sourced tephra is defined as pre-dating deposition of Vilcún Tephra at *c.* 850 cal. a BP and post-dating the deposition of the Michimahuida-sourced Lepué Tephra

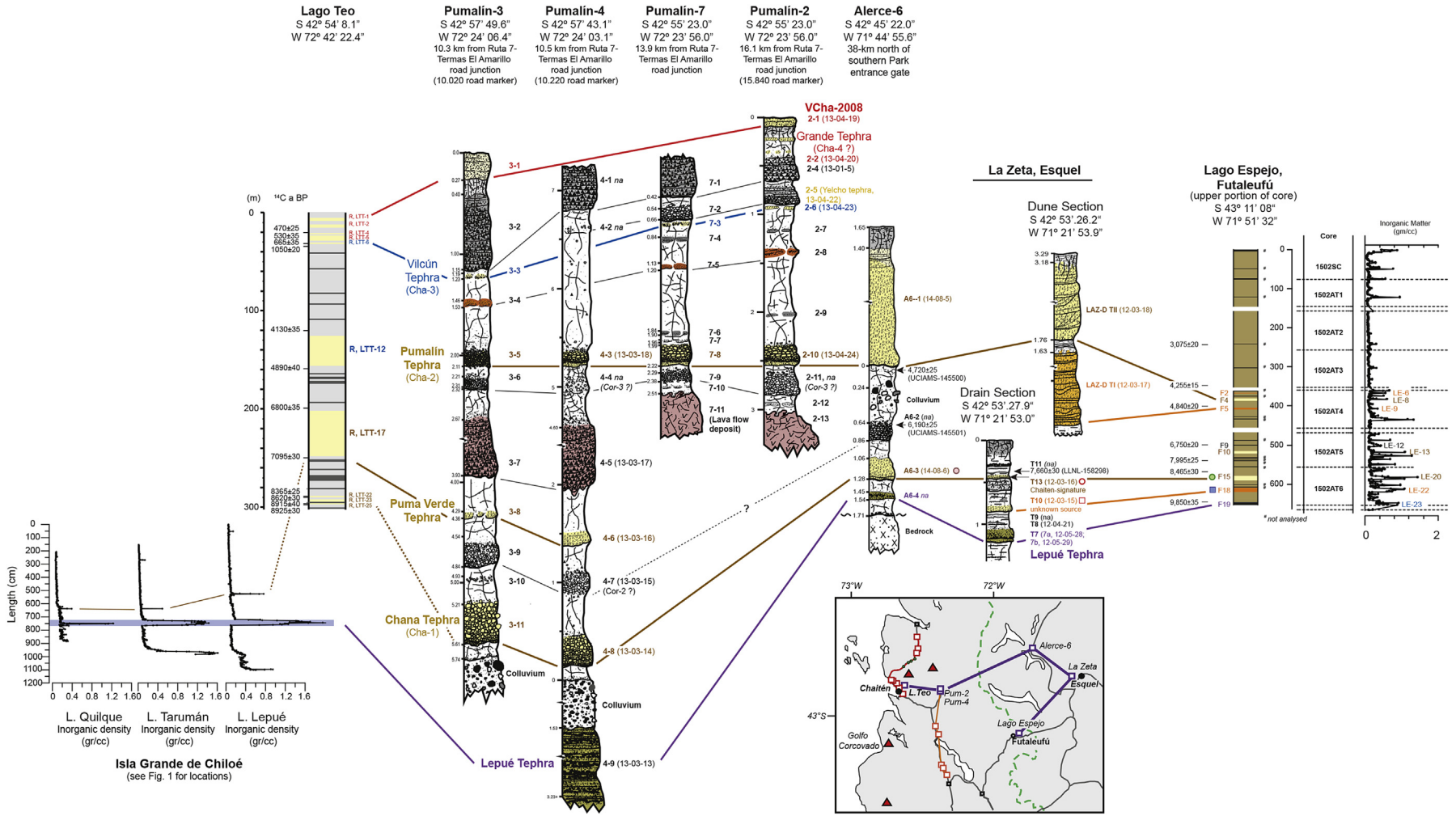

Fig. 4. Stratigraphic columns showing the correlation of the middle set of VCha-sourced tephra (pre-850 and post-11,000 cal a BP) from sediment cores retrieved from lakes (Quilque, Tarumán and Lepué) located on Isla Grande de Chiloe, Lago Teo (Moreno et al., 2015b), Pumalín-3, -4, -7 and -2 in the south-east sector, Alerce-6 located distally eastwards in Alerce Parque Nacional in Argentina, La Zeta sections located close to Esquel and Lago Espejo located ~72 km south east of VCha in the vicinity of Futaleufú. Red, blue and brown line designations indicate VCha-sourced tephra of 'young', 'mixed' and 'old' magma type, respectively. Purple colour highlights Lepué Tephra from MimVC (see also Alloway et al., 2017). For Lago Teo and Lago Espejo, yellow layers indicate rhyolitic tephra of VCha-source, black indicates tephra of likely MimVC-source and orange represent rhyolitic tephra from yet-to-be-determined eruptive sources. Colour-coded numeric designations for tephra (and sample numbers) along with the position of radiocarbon dates (presented as ^{14}C a BP) are also indicated alongside each described reference section. (For interpretation of the references to colour in this figure legend, the reader is referred to the web version of this article.)

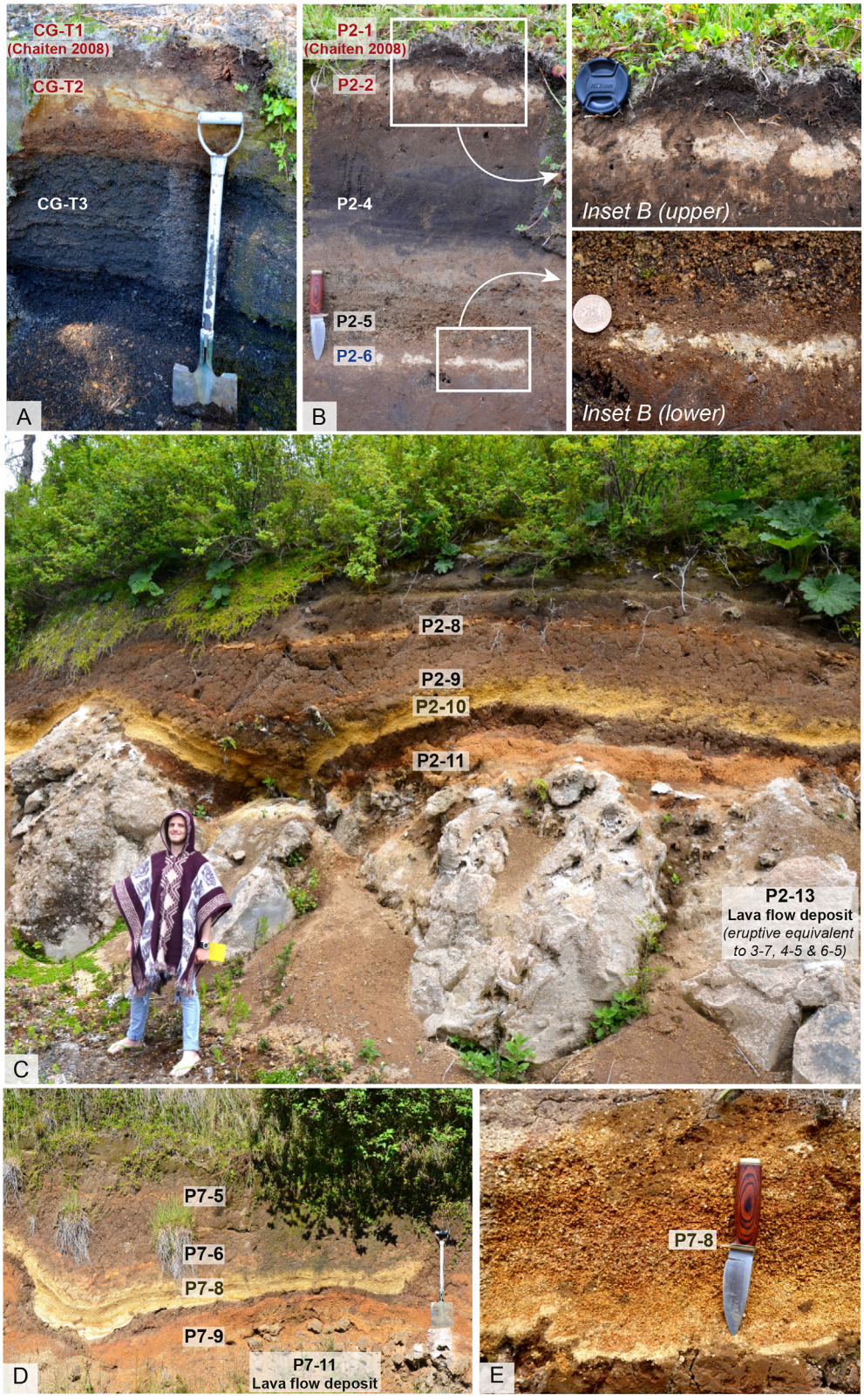

Fig. 5. The stratigraphies exposed at Campo Grande **(A)**, Pumalín-2 **(B, C)** and Pumalín-7 **(D)** showing VCha-sourced tephra interbedded with andic soil material and other tephra sourced predominantly from the MimVC. Red, blue and brown colour coding indicates VCha-sourced tephra of young, mixed and old magma type, respectively. **Inset B (upper)** shows the VCha-2008 tephra (P2-1) dispersed on the ground surface and closely underlain by Grande Tephra (P2-2). **Inset B (lower)** shows Vilcún Tephra (P2-6) closely overlain by a distinct bed of brown pumiceous lapilli (P2-5, informally named Yelcho tephra) likely sourced from a valley nested subsidiary dome located immediately southwest of VCha. Note in **C** the occurrence of Pumalín Tephra (P2-10) closely overlying a lava-flow deposit sourced from an isolated MimVC monogenetic cone perched on the elevated flank of an ice-sculptured basement range immediately west of the Río Michimahuida (S 42° 56′ 18.75″ S; W 72° 24′ 45.22″); **(5E)** – shows the typical internal bedding architecture of Pumalín Tephra (P7-8) at Pumalín -7. (For interpretation of the references to colour in this figure legend, the reader is referred to the web version of this article.)

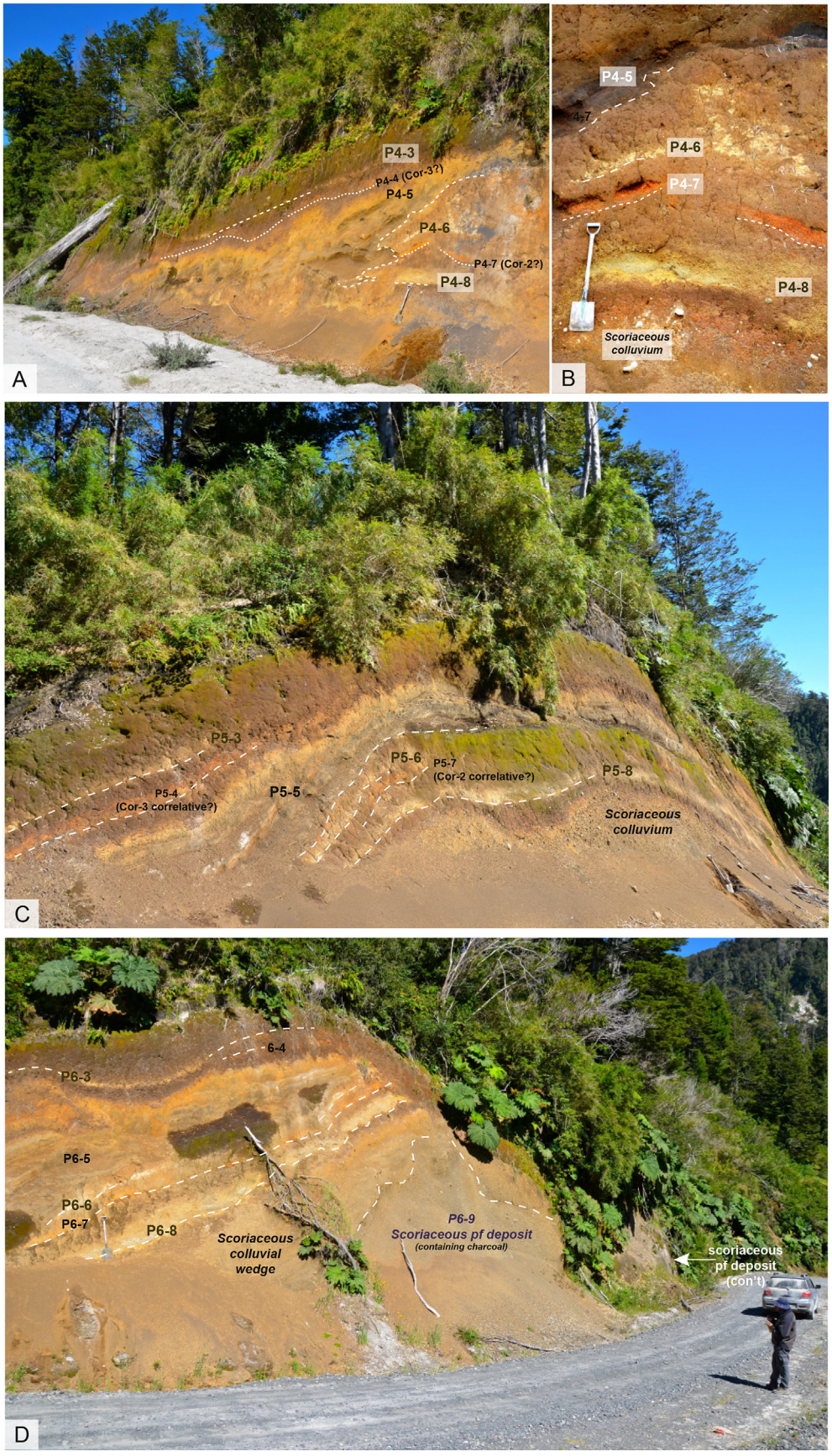

Fig. 6. The stratigraphies exposed at Pumalín-4 **(A, B)**, Pumalín-5 **(C)** and Pumalín-6 **(D)** showing Pumalín, Puma Verde and Chana Tephras (all of 'old' magma type) interbedded with andic soil material and other tephra sourced predominantly from the MimVC. Chana Tephra (P4-8, P5-8 and P6-8) closely overlies colluvial wedges resting on scoriaceous pyroclastic flow debris of Amarillo Ignimbrite (Amigo et al., 2013; Alloway et al., 2017).

Fig. 7. A. Massive bedded, moderately-sorted Puma Verde Tephra at Pumalín-6; **B.** Shower bedded Chana Tephra at Pumalin-4 overlying well pedologically structured, andic soil material developed into colluvium below; **C.** The occurrence of Chana Tephra exposed at the base of >20 m high cliffs on the northern side of the Río Raya. Here, an erosional sequence of dominantly massive to graded (reverse to normal), very coarse-grained (non-cohesive) hyperconcentrated and debris flow deposits overlie carbonaceous silts and sands with trees in position of growth. The lowermost debris flow in this sequence is reverse-graded, contains oriented tree moulds and is dominated by angular clasts of coarse pumiceous lapilli to block size (cf. debris flows occurring higher in the sequence); **i)** Erosional relief on the pumiceous (Chana Tephra) debris flow deposit caused by a subsequent debris flow event; **ii)** Flame structure at the basal contact of the lowermost debris flow deposit that indicates rapid deposition on a saturated soft sediment ground surface; **iii)** Radiocarbon samples (UCIAMS-122957 and -122958) were obtained from organic muds and wood in position of growth immediately underlying the pumiceous debris flow deposit. Radiocarbon ages of 8525 ± 30 (mud) and 9600 ± 25 (wood) ^{14}C a BP were retrieved and are broadly in accord with the *c.* 8700 ^{14}C a BP age of Cha-1 (Watt et al., 2011).

at *c.* 11,000 cal a BP (Alloway et al., 2017). In a sequence of well-exposed roadside sections occurring along W-887 in the south-eastern sector of Volcán Michimahuida, three prominent rhyolitic ash and lapilli layers are persistently observed within the andic cover-bed sequence (see Fig. 4). The uppermost tephra of this 'middle grouping' (here formally named Pumalín Tephra) can be observed in Pumalín-2 (P2-T10), -3 (P3-T5), -4 (P4-T3) and -7 (P7-T8). At these localities, Pumalín Tephra comprises a compact 1–2-cm thick basal sub-layer of pale yellow-brown fine to medium ash overlain by a decimetre-thick yellow-brown reverse-graded fine to coarse pumiceous lapilli bed exhibiting shower bedding. This lapilli closely overlies a strongly weathered reddish-brown pumiceous lapilli bed (e.g. Pum-3-6, Pum-4-4, Pum-7-9, Pum-2-11; tentatively correlated with Cor-3 of Naranjo and Stern, 2004) which in turn closely overlies a prominent agglutinated lava flow deposit (P7-11, P2-13; see Fig. 5C, D and E) and/or its co-eruptive scoriaceous fall deposits (P3-T7, P4-T5) sourced from an isolated MimVC monogenetic spatter cone perched on the elevated flank of an ice-sculptured basement range immediately west of the Río Michimahuida (S 42° 56′ 18.75″ S; W 72° 24′ 45.22"). A small lake of unknown depth now occupies the spatter cone crater. Pumalín Tephra can be correlated with Cha-2 tephra of Watt et al. (2013b) dated at 5013 ± 111 cal a BP. On the western side of the Andes and proximal to source, Pumalín Tephra is typically enveloped by andic soil material of medial to medial-ashy grade that shows the highest degree of soil development (*cf.* andic soil material formed over other intervals of the Holocene) and is reflected by its fine blocky structure, friability and intense reddish-brown chromas. However, in drier eastern Andean sites (i.e. La Zeta, Argentina; see Fig. 4), prominent aeolian dune sets sometimes separated by a weakly developed paleosol can be observed comprised dominantly of coarse-grained pumiceous ashy constituents of Pumalín Tephra (LAZ-DII) and an underlying pumiceous rhyolite tephra of unknown origin (i.e. LAZ-DI, Cor-3 correlative?).

At Pumalín-3, -4, -5 and -6 sections (Figs. 4 and 6) scoriaceous fall deposits from the valley-flanking MimVC monogenetic spatter cone separates Pumalín Tephra above, from a compact, pale brown, poorly sorted, crudely stratified, rhyolitic fine to coarse ash below, which has common, medium angular pumiceous lapilli dispersed in ashy matrix concentrated at its base (i.e. P3-T8, P4-T6, P5-T6 and P6-6) (Fig. 7A). This tephra (here formally named Puma Verde Tephra) closely overlies a strongly weathered, orange lapilli bed (i.e. P3-T9, P4-T7, P5-T7 and P6-T7) that is tentatively correlated with Cor-2 of Naranjo and Stern (2004). Although Puma Verde Tephra is conspicuous in proximal cover-bed sections, it is not macroscopically discernible within andic soil sequences of the eastern Andes (though it can be identified as a 1-cm thick fine vitric ash (F10) within the Lago Espejo sediment core; see Fig. 4 and Table 2). A rhyolitic cryptotephra correlative of similar age (*c.* 8300 cal. a BP) is prominently represented by an inorganic density peak at ~600-cm depth within sediment cores retrieved from Lago Quilque (P.I. Moreno, *unpublished data*), Lago Tarumán (Gonzalorena Vallejos, 2014), Lago Lepué (Pesce and Moreno, 2014) on Isla Grande de Chiloé (see Fig. 4).

Closely underlying Puma Verde Tephra in proximal southeastern sectors of MimVC, is a prominent shower-bedded rhyolitic ash and lapilli bed (P3-T11, P4-T8, P5-T8, P6-T8; here formally named Chana Tephra) which intervenes between Cor-2 correlative above, and colluvium draping the *c.* 11,000 cal a BP Lepué Tephra below (Figs. 4 and 6; Alloway et al., 2017). Chana Tephra can be observed in Pumalín-3 (P3-T11) and -4 (P4-T8) where it typically comprises a ~8 cm-thick thick bed of fine pumiceous ash overlain by a ~26 cm thick bed of bright yellow-brown, shower-bedded, coarse to very coarse pumiceous ash and very fine lapilli (Fig. 7B). Further eastwards at Alerce-6 and La Zeta sections, Chana Tephra exhibits a similar bedding architecture with a fine ash basal bed (~1–2 cm) overlain by a much thicker (~6-cm) massive to faintly normal bedded medium to coarse pumiceous ash. At La Zeta, intervening between Chana Tephra above and Lepué Tephra below, is a ~5-cm thick fine to very fine white vitric ash (LZ-T10) (Fig. 4). The glass chemistry of LZ-T10 is quite distinctive from that of interpreted VCha-source with glass shard chemistries similar to those of LAZ-DT1 and LAZ–T1 also occurring within the La Zeta section (see Figs. 4 and 8). At present, the eruptive source of these three tephra layers is unknown.

Two roadside sections in the northwest sector of VCha facilitate field correlation to Cha-1 (*sensu stricto*) as it was originally described and defined by Naranjo and Stern (2004). At Sections 4 (S4) and 5 (S5) situated on Ruta 7 north of Chaitén township (see Fig. 1), a prominent metre (m)-thick, rhyolitic pumiceous lapilli closely overlies a scoriaceous fall and surge co-eruptive couplet sourced from Volcán Michimahuida (now referred to as Lepué Tephra: Alloway et al., 2017) (Fig. 4). At S4, Lepué Tephra was dated at 11,483 ± 1034 cal a BP (9960 ± 330 ^{14}C a BP) and is indistinguishable in its stratigraphic position, age and constituent major- and trace-element glass chemistry from Lepué Tephra and its co-eruptive Amarillo Ignimbrite occurring in sections south-east of Volcán Michimahuida (Alloway et al., 2017). On this basis, Cha-1 at these sections can be confidently correlated with Chana Tephra (this study) described from Pumalín-3, -4 (see Fig. 4), -5 and -6) (see Figs. 6 and 7) which typically occurs closely overlying colluvium sitting on a decimetre-thick scoriaceous pyroclastic flow deposit (Amarillo Ignimbrite; Amigo et al., 2013; Alloway et al., 2017).

The only other observed near-proximal occurrence of Cha-1 (Chana Tephra) in the north-west sector is exposed at the base of >20 m high cliffs on the northern side of the Río Raya (Fig. 7C and insets). Here, a sequence of dominantly massive to graded (reverse to normal), very coarse-grained (non-cohesive) hyperconcentrated and debris flow deposits overlie carbonaceous silts and sands containing trees in position of growth. The lowermost debris flow in this sequence is reverse-graded, contains oriented tree moulds and is dominated by angular clasts of coarse pumiceous lapilli and blocks (*cf.* lithic dominated debris flows occurring higher in the sequence). Flame structures were observed at the basal contact of the lowermost debris flow deposit and indicate rapid deposition on a saturated ground surface. Two radiocarbon samples (UCIAMS-122957 and -122958) were obtained from the underlying organic mud and wood in position of growth that yielded ages of 8525 ± 30 and 9600 ± 25 ^{14}C a BP respectively. These ages are broadly in accord with the *c.* 8700 ^{14}C a BP age of Cha-1 (Watt et al., 2011). The occurrence of this pumice-bearing debris flow deposit likely indicates landscape instability in the aftermath of the Cha-1 eruption. Correlation of debris-flow pumice constituents to Cha-1/Chana Tephra occurring in south-east sectors are further discussed in the tephra geochemistry section below.

Within the Lago Teo sediment core between *c.* 850 and 11,000 cal a BP, five VCha-sourced rhyolitic ash layers were recognised (LTT-12, -17, -23, -24 and -25; Moreno et al., 2015b). Of these, LTT-12 and -17 occurring in the middle portions of the core (~130- to 250-cm depth) have maximum ages of *c.* 5600 and 7900 cal a BP, respectively, and are very prominently represented as decimetre-to centimetre-thick vitric-rich fine to coarse ash beds. LTT-23, -24 and -25 occur towards the base of the core (~290–300 cm) as closely spaced, cm-thick, fine-coarse ash layers. These three tephra are well dated and constrained in age between 9600 and 10,200 cal a BP (*c.* 9462, *c.* 9592 and *c.* 9678 cal. a BP, respectively).

The greater number of tephra preserved within lake sediments compared with those tephra recognised within andic cover-beds (Pumalín, Puma Verde and Chana Tephras) over the same time period provides an indication of the difficulty in accurately

Table 2
Summary of normalised (to an anhydrous basis) glass shard major-element compositions of tephra beds from VCha, MimVC and unknown eruptive sources in the Chaitén, Chiloé & Esquel Sectors. Red, blue and brown colours indicate 'young', 'mixed' and 'old' VCha magma types; Orange indicates possible derivation from the newly recognised satellite dome adjacent to VCha; Black colours indicate likely MimVC-source, purple colour highlights Lepué Tephra from MimVC (see also Alloway et al., 2017) and green colour represents tephra from yet-to-be-determined eruptive sources.

Section	Tephra	Sample	Probe Run	SiO_2	Al_2O_3	TiO_2	FeO	MgO	MnO	CaO	Na_2O	K_2O	Cl	H_2O	*n*
	VCha-2008[1]			75.98 (0.45)	14.05 (0.26)	0.12 (0.02)	1.27 (0.11)	0.26 (0.04)	0.06 (0.02)	1.26 (0.13)	3.86 (0.24)	3.14 (0.20)	nd	1.50 (1.62)	250
Section 11 (Fig. 2)	Grande	11-7 (12-07-9)	July 17, 2012	75.81 (0.15)	14.00 (0.14)	0.13 (0.02)	1.31 (0.08)	0.25 (0.02)	0.05 (0.03)	1.31 (0.03)	4.06 (0.10)	3.00 (0.08)	0.09 (0.01)	-0.41 (0.76)	20
	Vilcún	11-6 (12-07-8)		76.42 (0.31)	13.75 (0.22)	0.10 (0.02)	1.19 (0.09)	0.21 (0.03)	0.06 (0.02)	1.21 (0.06)	3.97 (0.19)	2.99 (0.11)	0.10 (0.01)	1.53 (1.52)	20
Puente Salvador Coma (Fig. 2)	Grande	pSC-5 (13-02-8)	April 16, 2013	75.85 (0.15)	13.92 (0.10)	0.13 (0.02)	1.28 (0.08)	0.24 (0.02)	0.06 (0.02)	1.33 (0.06)	4.09 (0.13)	3.02 (0.06)	0.08 (0.01)	-0.67 (0.42)	18
		pSC-4 (13-02-9)		76.29 (0.60)	13.75 (0.23)	0.12 (0.02)	1.26 (0.15)	0.22 (0.06)	0.05 (0.03)	1.27 (0.11)	3.88 (0.34)	3.08 (0.16)	0.09 (0.01)	2.00 (2.02)	18
	Vilcún	pSC-3 (13-02-10)		76.51 (0.37)	13.60 (0.17)	0.10 (0.02)	1.19 (0.10)	0.20 (0.03)	0.06 (0.02)	1.14 (0.14)	3.99 (0.10)	3.12 (0.10)	0.10 (0.02)	-0.26 (0.66)	16
		pSC-2 (13-02-11)		76.41 (0.36)	13.68 (0.25)	0.10 (0.02)	1.22 (0.09)	0.21 (0.03)	0.06 (0.02)	1.21 (0.10)	3.96 (0.16)	3.05 (0.11)	0.10 (0.01)	0.69 (0.48)	16
Puente Raya - 0.5 km (south) (Fig. 2)	Grande	PR-up (15-02-1)	May 8, 2015	75.89 (0.47)	14.07 (0.35)	0.14 (0.02)	1.36 (0.10)	0.27 (0.02)	0.05 (0.02)	1.40 (0.15)	3.72 (0.18)	3.01 (0.16)	0.08 (0.01)	0.05 (0.70)	25
	Vilcún	PR-lwr (15-02-2)		76.52 (0.49)	13.73 (0.22)	0.12 (0.02)	1.22 (0.11)	0.22 (0.05)	0.06 (0.02)	1.26 (0.15)	3.69 (0.16)	3.08 (0.13)	0.09 (0.02)	0.65 (1.15)	23
Lago Pinto, Futaleufú (Fig. 2)	VCha-2008	LP-T1 (15-01-6)	May 8, 2015	75.77 (0.32)	14.11 (0.21)	0.15 (0.01)	1.35 (0.08)	0.27 (0.02)	0.06 (0.02)	1.45 (0.09)	3.76 (0.13)	3.00 (0.09)	0.09 (0.01)	0.51 (0.71)	24
	MimVC	LP-T2 (15-01-1)		56.22 (0.63)	14.17 (0.54)	2.62 (0.18)	11.37 (0.48)	3.33 (0.31)	0.22 (0.04)	6.76 (0.42)	3.50 (0.22)	1.72 (0.16)	0.10 (0.01)	0.02 (0.88)	24
		LP-T3 (15-01-2)		75.93 (0.20)	14.01 (0.12)	0.14 (0.01)	1.37 (0.07)	0.28 (0.02)	0.07 (0.03)	1.38 (0.06)	3.74 (0.10)	2.99 (0.10)	0.10 (0.01)	0.38 (1.48)	24
		LP-T4 (15-01-3)		75.86 (0.27)	14.05 (0.20)	0.14 (0.01)	1.34 (0.08)	0.27 (0.03)	0.06 (0.02)	1.42 (0.07)	3.76 (0.14)	3.00 (0.09)	0.11 (0.06)	1.28 (1.79)	24
		LP-T5 (15-01-4)		67.24 (0.39)	15.41 (0.36)	0.75 (0.05)	5.22 (0.22)	0.80 (0.08)	0.14 (0.02)	2.73 (0.22)	4.37 (0.19)	3.18 (0.15)	0.16 (0.02)	0.20 (1.15)	21
	Vilcún	LP-T6 (15-01-5)		76.51 (0.60)	13.78 (0.41)	0.11 (0.02)	1.19 (0.13)	0.21 (0.03)	0.06 (0.02)	1.28 (0.23)	3.71 (0.21)	3.06 (0.16)	0.09 (0.02)	0.26 (0.99)	25
Pumalín-2 (Fig. 4)	VCha-2008	2-1 (13-04-19)	April 19, 2013	75.71 (0.18)	13.98 (0.11)	0.13 (0.02)	1.34 (0.05)	0.26 (0.03)	0.05 (0.02)	1.37 (0.03)	4.07 (0.14)	3.00 (0.07)	0.09 (0.01)	0.34 (0.84)	17
	Grande	2-2 (13-04-20)		75.82 (0.19)	13.95 (0.11)	0.12 (0.02)	1.33 (0.09)	0.25 (0.02)	0.07 (0.02)	1.34 (0.03)	4.04 (0.13)	2.99 (0.07)	0.08 (0.01)	-1.09 (0.88)	18
		2-3 (13-04-21)	Ant-nest Pop. 1	75.66 (0.20)	13.99 (0.10)	0.13 (0.02)	1.39 (0.09)	0.25 (0.02)	0.06 (0.02)	1.34 (0.07)	4.06 (0.15)	3.03 (0.11)	0.08 (0.01)	-0.86 (0.71)	11
			Pop. 2	54.18 (0.87)	15.20 (0.19)	1.75 (0.17)	10.32 (0.50)	5.05 (0.76)	0.20 (0.02)	8.21 (0.90)	3.82 (0.50)	1.20 (0.32)	0.09 (0.02)	-0.74 (0.53)	8
	MimVC	2-4 (13-01-5)	April 16, 2013	53.22 (0.50)	14.80 (0.35)	1.69 (0.11)	10.64 (0.74)	5.93 (0.37)	0.19 (0.07)	9.60 (0.39)	3.08 (0.26)	0.78 (0.21)	0.08 (0.03)	-0.48 (0.58)	17
		2-5 (13-04-22)	April 19, 2013	66.82 (0.28)	15.45 (0.18)	0.70 (0.03)	5.37 (0.17)	0.81 (0.05)	0.14 (0.02)	2.74 (0.09)	4.73 (0.16)	3.10 (0.11)	0.15 (0.02)	-2.04 (0.48)	17
	Vilcún	2-6 (13-04-23)		76.32 (0.38)	13.72 (0.24)	0.10 (0.02)	1.20 (0.11)	0.19 (0.04)	0.05 (0.02)	1.22 (0.12)	4.06 (0.18)	3.05 (0.12)	0.09 (0.01)	0.78 (0.59)	19
	Pumalín	2-10 (13-04-24)		77.01 (0.40)	13.36 (0.24)	0.09 (0.02)	1.20 (0.11)	0.16 (0.03)	0.07 (0.02)	0.96 (0.12)	3.84 (0.13)	3.22 (0.13)	0.08 (0.01)	1.07 (1.95)	16
Pumalín-4 (Fig. 4)	Pumalín	4-3 (13-03-18)	April 19, 2013	76.96 (0.42)	13.38 (0.26)	0.09 (0.02)	1.21 (0.15)	0.16 (0.05)	0.06 (0.02)	0.96 (0.13)	3.88 (0.15)	3.22 (0.20)	0.08 (0.02)	0.00 (1.88)	19
		4-5 (13-03-17)		53.44 (1.04)	14.97 (0.28)	1.61 (0.09)	10.39 (0.85)	5.17 (0.46)	0.20 (0.02)	9.34 (0.65)	3.52 (0.15)	1.23 (0.10)	0.12 (0.03)	-1.81 (0.83)	13
	Puma Verde	4-6 (13-03-16)		76.79 (0.15)	13.48 (0.10)	0.10 (0.02)	1.19 (0.06)	0.17 (0.01)	0.07 (0.02)	1.02 (0.03)	3.95 (0.12)	3.15 (0.09)	0.08 (0.01)	-1.02 (0.46)	20
		4-7 (13-03-15)		64.30 (0.74)	16.53 (0.50)	0.66 (0.02)	5.67 (0.65)	1.45 (0.42)	0.17 (0.04)	4.73 (0.34)	5.12 (0.20)	1.22 (0.05)	0.15 (0.02)	-1.40 (1.21)	3
	Chana (Cha-1 corr)	4-8 (13-03-14)		77.44 (0.56)	13.35 (0.23)	0.08 (0.02)	1.27 (0.09)	0.18 (0.03)	0.06 (0.02)	0.98 (0.11)	3.48 (0.36)	3.06 (0.17)	0.09 (0.01)	4.77 (1.04)	16
		4-9 (13-03-13)		54.82 (1.17)	15.64 (0.43)	2.10 (0.36)	9.85 (0.86)	4.14 (0.56)	0.19 (0.03)	7.32 (0.53)	3.74 (0.61)	2.11 (1.20)	0.09 (0.03)	0.58 (0.23)	5
Alerce-6 (Fig. 4)	Pumalín	Alerce-1 (14-08-5)	Sept. 17 2015	76.39 (0.14)	13.86 (0.07)	0.11 (0.01)	1.30 (0.08)	0.24 (0.02)	0.06 (0.02)	1.25 (0.03)	3.69 (0.11)	2.99 (0.11)	0.11 (0.01)	3.55 (1.17)	25
	Chana	Alerce-3 (14-08-6)		76.45 (0.18)	13.87 (0.12)	0.10 (0.02)	1.35 (0.09)	0.21 (0.03)	0.06 (0.02)	1.21 (0.05)	3.65 (0.11)	3.00 (0.12)	0.10 (0.03)	4.29 (1.19)	25

Campo Grande (Fig. 5)	**MimVC**	**CG-T3** (13-01-6)	*April 16, 2013*	54.42 (0.32)	14.90 (0.25)	1.77 (0.08)	10.21 (0.35)	5.29 (0.19)	0.21 (0.03)	8.51 (0.20)	3.53 (0.25)	1.09 (0.05)	0.08 (0.01)	0.23 (0.56)	17
Río Raya (Fig. 7)	**Chana**	**Raya-1** (13-02-7)	*April 16, 2013*	76.18 (0.17)	13.81 (0.08)	0.10 (0.04)	1.39 (0.09)	0.20 (0.01)	0.06 (0.02)	1.19 (0.03)	4.10 (0.10)	2.87 (0.08)	0.10 (0.01)	1.64 (0.87)	20
Paso de Lago Blanco (S-4) (Fig. 8)	**Cha-1** *(sensu stricto;* Chana Tephra)	**Upper** (14-11-1)	*Oct 31, 2015*	76.70 (0.19)	13.92 (0.09)	0.07 (0.03)	1.27 (0.11)	0.22 (0.02)	0.06 (0.02)	1.17 (0.17)	3.71 (0.11)	2.79 (0.08)	0.11 (0.01)	2.09 (0.97)	23
		Lower (14-11-3)		76.40 (0.29)	13.94 (0.11)	0.08 (0.03)	1.42 (0.10)	0.21 (0.02)	0.06 (0.04)	1.06 (0.24)	3.79 (0.17)	2.92 (0.13)	0.11 (0.02)	4.07 (1.14)	23
	Lepué	**14J13S4-3** (13-06-33)	*April 19, 2013*	69.12 (2.06)	14.51 (0.39)	0.49 (0.15)	4.48 (0.72)	0.51 (0.30)	0.16 (0.04)	2.16 (0.96)	5.06 (0.22)	3.34 (0.31)	0.17 (0.03)	-1.88 (1.09)	17
		14J13S4-2 (13-06-32)		71.23 (0.28)	14.19 (0.10)	0.34 (0.03)	3.70 (0.18)	0.23 (0.03)	0.14 (0.02)	1.38 (0.07)	5.06 (0.15)	3.54 (0.08)	0.19 (0.01)	-0.84 (0.46)	18
	rhyolitic breccia (VCha)	**14J13S4-1** (13-06-31)		76.76 (0.33)	13.53 (0.24)	0.06 (0.02)	1.23 (0.08)	0.13 (0.02)	0.07 (0.02)	1.04 (0.08)	3.96 (0.16)	3.15 (0.12)	0.07 (0.01)	-1.09 (0.47)	20
Puente Águila (S-5) (Fig. 8)	**Lepué**	**14J13S5-1** (13-06-35)	*April 19, 2013*	71.32 (0.45)	14.15 (0.16)	0.33 (0.04)	3.74 (0.16)	0.21 (0.04)	0.14 (0.02)	1.36 (0.11)	4.98 (0.16)	3.58 (0.13)	0.19 (0.02)	-1.14 (1.00)	16
El Campo Lago Blanco (S-6) (Fig. 8)	**rhyolitic breccia** (VCha)	**6-5** (12-06-5)	*Jul. 16, 2012*	76.27 (0.87)	13.62 (0.55)	0.10 (0.02)	1.28 (0.29)	0.18 (0.08)	0.07 (0.03)	1.10 (0.25)	4.07 (0.40)	3.26 (0.25)	0.07 (0.01)	-0.83 (0.79)	18
	VCha-fall	**6-4** (12-06-4)		76.73 (0.30)	13.50 (0.19)	0.07 (0.01)	1.25 (0.08)	0.14 (0.02)	0.07 (0.02)	1.02 (0.08)	3.99 (0.14)	3.16 (0.09)	0.08 (0.01)	-0.72 (0.92)	22
	VCha-fall	**6-3** (12-06-3)		76.53 (0.32)	13.57 (0.14)	0.09 (0.01)	1.30 (0.27)	0.16 (0.07)	0.08 (0.03)	1.06 (0.07)	3.89 (0.12)	3.24 (0.11)	0.08 (0.02)	0.05 (1.74)	17
	VCha-PDC	**6-2** (12-06-2)		76.59 (1.18)	13.66 (0.76)	0.07 (0.02)	1.24 (0.24)	0.12 (0.05)	0.07 (0.03)	1.22 (0.35)	3.84 (0.46)	3.10 (0.34)	0.09 (0.02)	4.25 (1.25)	17
	VCha-fall	**6-1** (12-06-1)		74.33 (3.60)	14.91 (2.41)	0.10 (0.03)	1.29 (0.28)	0.20 (0.07)	0.07 (0.02)	1.85 (1.10)	4.41 (0.94)	2.80 (0.71)	0.05 (0.03)	0.84 (2.04)	21
Chaitén Disco (S-7) (Fig. 8)	**VCha**	**7-1** (12-06-6)		76.53 (0.43)	13.59 (0.25)	0.07 (0.02)	1.29 (0.12)	0.12 (0.03)	0.09 (0.02)	1.15 (0.09)	3.96 (0.16)	3.13 (0.10)	0.08 (0.01)	-0.28 (0.95)	21
Santa Lucía-2 (Fig. 8)	**VCha**	**StL-2** (15-02-6)	*May 8, 2015*	77.02 (0.13)	13.55 (0.09)	0.07 (0.02)	1.24 (0.07)	0.16 (0.02)	0.08 (0.02)	1.09 (0.03)	3.57 (0.08)	3.14 (0.07)	0.08 (0.01)	0.96 (1.31)	23
La Zeta, Esquel, ARG (Figs. 4 and 8)	**Pumalín**	**LAZ-D TII** (12-03-18)	*July 16, 2012*	76.29 (0.35)	13.76 (0.12)	0.11 (0.01)	1.38 (0.11)	0.22 (0.02)	0.04 (0.02)	1.19 (0.03)	3.94 (0.35)	2.96 (0.07)	0.10 (0.01)	2.09 (1.03)	15
	Unk	**LAZ-D TI** (12-03-17)		72.55 (0.16)	15.02 (0.11)	0.16 (0.02)	3.45 (0.15)	0.24 (0.01)	0.14 (0.03)	2.09 (0.05)	4.62 (0.16)	1.53 (0.05)	0.19 (0.04)	2.01 (2.25)	11
	Chana	**LAZ-T13** (12-03-16)		76.21 (0.27)	13.85 (0.13)	0.09 (0.01)	1.39 (0.13)	0.21 (0.02)	0.08 (0.02)	1.16 (0.03)	3.96 (0.15)	2.95 (0.15)	0.10 (0.01)	3.10 (1.07)	22
	Unk	**LAZ-T10** (12-03-15)		70.13 (0.58)	15.77 (0.19)	0.27 (0.03)	4.07 (0.28)	0.42 (0.05)	0.14 (0.03)	2.45 (0.14)	4.88 (0.36)	1.67 (0.06)	0.20 (0.02)	-0.14 (1.55)	18
	MimVC	**LAZ-T8** (12-04-21)	*June 26, 2012*	55.21 (0.66)	15.51 (0.56)	1.86 (0.14)	10.35 (0.42)	3.99 (0.28)	nd	6.41 (0.29)	4.91 (0.23)	1.75 (0.14)	nd	-0.69 (0.58)	21
	Lepué - MimVC	**LAZ-T7B** (12-05-29)	*July 16, 2012*	71.14 (0.44)	14.30 (0.51)	0.32 (0.03)	3.73 (0.27)	0.19 (0.02)	0.14 (0.02)	1.36 (0.18)	5.27 (0.45)	3.35 (0.48)	0.21 (0.02)	-0.26 (0.94)	12
		LAZ-T7A (12-05-28)		71.38 (0.29)	14.17 (0.17)	0.33 (0.01)	3.68 (0.09)	0.20 (0.01)	0.15 (0.01)	1.28 (0.04)	5.00 (0.18)	3.60 (0.07)	0.21 (0.01)	-0.21 (1.35)	18
	VCha	**LAZ-T3** (12-03-14)		77.93 (1.81)	12.93 (1.11)	0.05 (0.02)	0.98 (0.23)	0.08 (0.04)	0.08 (0.02)	0.86 (0.33)	3.71 (0.63)	3.28 (0.32)	0.09 (0.02)	4.09 (1.07)	14
	VCha	**LAZ-T2** (12-04-19)	*June 26, 2012*	77.01 (0.78)	14.09 (0.22)	0.05 (0.03)	1.38 (0.16)	0.18 (0.04)	nd	1.09 (0.11)	3.18 (0.41)	3.02 (0.27)	nd	1.50 (1.32)	20
	Unk	**LAZ-T1** (12-03-13)	*July 16, 2012*	66.57 (0.73)	16.52 (0.53)	0.43 (0.05)	5.48 (0.58)	0.99 (0.13)	0.19 (0.02)	3.83 (0.28)	4.69 (0.21)	1.14 (0.11)	0.15 (0.02)	0.94 (1.21)	6
				72.33 (0.15)	15.02 (0.09)	0.17 (0.02)	3.46 (0.13)	0.25 (0.01)	0.15 (0.03)	2.16 (0.07)	4.69 (0.18)	1.59 (0.04)	0.20 (0.07)	4.47 (3.27)	10
	VCha	**LAZ-T12** (12-04-24)	*June 26, 2012*	77.71 (0.56)	13.89 (0.39)	0.04 (0.03)	1.38 (0.23)	0.11 (0.05)	nd	1.09 (0.10)	2.95 (0.36)	2.82 (0.34)	nd	2.39 (1.25)	16
	VCha	**JT-3** (14-10-1)		75.23 (0.54)	14.33 (0.44)	0.11 (0.02)	1.67 (0.20)	0.28 (0.09)	0.08 (0.03)	1.57 (0.19)	3.71 (0.24)	2.93 (0.12)	0.08 (0.01)	2.64 (1.27)	18
Lago Espejo, Futaleufú (Figs. 4 and 8)	**Unk**	**1502AT4,** 9-10-cm (16-07-F2)	*May 6, 2016*	62.73 (2.90)	15.34 (0.63)	1.47 (0.33)	7.14 (1.91)	2.46 (0.75)	0.14 (0.06)	4.88 (0.86)	4.15 (0.47)	1.53 (0.16)	0.16 (0.03)	1.04 (1.19)	20
	Pumalín	**1502AT4,** 25-26-cm (16-07-F4)		76.87 (0.38)	13.57 (0.22)	0.08 (0.04)	1.14 (0.13)	0.23 (0.12)	0.05 (0.05)	1.06 (0.13)	3.55 (0.34)	3.36 (0.21)	0.09 (0.08)	3.46 (2.55)	22
	Unk	**1502AT4,** 50-51-cm (16-07-F5)		67.09 (0.48)	16.09 (0.15)	1.19 (0.07)	3.77 (0.25)	1.34 (0.14)	0.15 (0.05)	2.43 (0.18)	4.72 (0.22)	3.08 (0.11)	0.13 (0.04)	1.83 (1.53)	22
	MimVC?	**1502AT5,** 43-44-cm (16-05-F9)		56.48 (0.40)	15.41 (0.40)	2.36 (0.15)	9.45 (0.46)	4.08 (0.16)	0.20 (0.08)	6.78 (0.10)	3.71 (0.33)	1.44 (0.05)	0.09 (0.01)	2.15 (0.83)	22
	Puma Verde	**1502AT5,** 61-62-cm		77.46 (0.56)	13.48 (0.32)	0.06 (0.03)	1.17 (0.11)	0.22 (0.07)	0.08 (0.05)	1.01 (0.11)	3.25 (0.23)	3.21 (0.15)	0.07 (0.01)	3.08 (1.73)	22

		(16-07-F10)													
	Chana	1502AT6, 25-29-cm (16-07-F15)		77.39 (0.41)	13.52 (0.15)	0.08 (0.05)	1.16 (0.19)	0.20 (0.10)	0.06 (0.05)	1.02 (0.05)	3.26 (0.25)	3.23 (0.16)	0.09 (0.02)	6.05 (1.02)	44
	Unk	1502AT6, 55-62-cm (16-07-F18)		70.64 (0.66)	15.81 (0.14)	0.27 (0.07)	3.91 (0.26)	0.49 (0.11)	0.14 (0.05)	2.57 (0.17)	4.31 (0.27)	1.71 (0.10)	0.16 (0.02)	1.85 (1.04)	20
	Lepué - MimVC	1502AT6, 89-90-cm (16-08-F19)		54.04 (0.47)	14.83 (0.31)	2.34 (0.09)	12.04 (0.35)	4.70 (0.19)	0.18 (0.06)	7.19 (0.18)	3.11 (0.25)	1.49 (0.07)	0.08 (0.01)	-1.60 (0.78)	22
	VCha	1502AT8, 5-14-cm (16-08-F20)		76.14 (0.31)	13.95 (0.16)	0.06 (0.04)	1.57 (0.21)	0.18 (0.08)	0.08 (0.05)	1.25 (0.06)	3.51 (0.24)	3.18 (0.14)	0.07 (0.01)	2.07 (1.24)	22
	VCha	1502AT8, 37-40-cm (16-08-F22)		76.46 (0.32)	13.91 (0.16)	0.06 (0.03)	1.38 (0.14)	0.20 (0.07)	0.06 (0.05)	1.24 (0.05)	3.49 (0.26)	3.12 (0.11)	0.07 (0.01)	2.11 (1.46)	22
	Unk	(1502AT9, 87-91-cm 16-08-F23)		72.72 (0.53)	15.19 (0.14)	0.17 (0.05)	3.31 (0.30)	0.36 (0.10)	0.15 (0.06)	2.37 (0.13)	4.08 (0.24)	1.52 (0.08)	0.13 (0.01)	3.26 (1.21)	21
Lago Pichilafquén (Figs. 14 and 15)	Cha-1	AT-3-T6 *(14-11-2)*	*Oct. 31, 2015*	76.43 (0.33)	13.86 (0.09)	0.09 (0.04)	1.46 (0.12)	0.20 (0.02)	0.05 (0.03)	1.05 (0.22)	3.67 (0.11)	3.09 (0.13)	0.09 (0.01)	4.62 (1.34)	*23*
Antillanca (Fig. 15)	Cha-1	Ant-1 (14-05-3)	*Sept. 12, 2014*	76.24 (0.32)	13.91 (0.18)	0.10 (0.01)	1.32 (0.07)	0.22 (0.02)	0.07 (0.02)	1.18 (0.09)	3.88 (0.19)	3.00 (0.10)	0.08 (0.01)	4.35 (1.16)	*22*
Ralun (Figs. 14 and 15)	Cha-1	(11-3-2)	*May 19, 2011*	76.65 (0.12)	13.98 (0.08)	0.09 (0.02)	1.27 (0.03)	0.21 (0.02)	0.07 (0.02)	1.07 (0.03)	3.57 (0.12)	3.08 (0.03)	nd	2.86 (0.87)	21
Puelche (Figs. 14 and 15)	Cha-1	8J13S2-T2 (13-05-29)	*April 19, 2013*	76.45 (0.23)	13.76 (0.14)	0.09 (0.02)	1.34 (0.16)	0.19 (0.04)	0.07 (0.02)	1.17 (0.04)	3.85 (0.13)	2.99 (0.10)	0.09 (0.01)	2.73 (1.39)	19
Cholgo (Figs. 14 and 15)	Cha-1	9J13S5-T2 (13-05-30)	*April 19, 2013*	76.30 (0.28)	13.78 (0.19)	0.10 (0.02)	1.38 (0.11)	0.20 (0.03)	0.07 (0.03)	1.18 (0.06)	3.89 (0.13)	3.03 (0.10)	0.09 (0.01	3.35 (1.95)	18
Subsidiary VCha Dome [#] (Fig. 18)		**Banded lava float**	*March 26, 2015*	65.78 (1.46)	16.90 (1.01)	0.47 (0.11)	3.72 (0.88)	1.60 (0.52)	0.08 (0.03)	4.42 (0.68)	4.15 (0.22)	2.85 (0.37)	0.02 (0.01)	1.33 (1.20)	21
Glass standards	VG-568		*June 26, 2012*	76.96 (0.38)	12.17 (0.09)	0.05 (0.03)	1.09 (0.14)	0.01 (0.01)	nd	0.45 (0.05)	3.52 (0.19)	4.93 (0.07)	nd	2.44 (0.46)	28
			March 26, 2015	76.92 (0.23)	12.17 (0.08)	0.08 (0.02)	1.08 (0.12)	0.02 (0.01)	0.02 (0.02)	0.45 (0.02)	3.52 (0.26)	4.93 (0.08)	0.07 (0.01)	0.74 (0.25)	10
	ATHO-G		*Jul 16, 2012*	75.57 (0.48)	12.20 (0.08)	0.25 (0.02)	3.32 (0.15)	0.10 (0.02)	0.10 (0.01)	1.70 (0.05)	3.78 (0.15)	2.64 (0.10)	0.05 (0.01)	0.29 (0.58)	18
			Jul. 17, 2.012	75.63 (0.38)	12.21 (0.24)	0.24 (0.01)	3.27 (0.14)	0.10 (0.01)	0.10 (0.01)	1.70 (0.04)	3.75 (0.21)	2.64 (0.07)	0.05 (0.01)	0.31 (0.68)	12
			Oct. 23, 2012	75.61 (0.41)	12.20 (0.08)	0.23 (0.02)	3.29 (0.10)	0.11 (0.01)	0.11 (0.02)	1.70 (0.02)	3.75 (0.15)	2.64 (0.04)	nd	0.37 (0.51)	123
			April 16, 2013	75.60 (0.45)	12.20 (0.10)	0.24 (0.02)	3.29 (0.12)	0.09 (0.01)	0.11 (0.02)	1.70 (0.10)	3.75 (0.17)	2.64 (0.06)	0.04 (0.01)	0.34 (0.55)	85
			April 19, 2013	75.61 (0.54)	12.20 (0.12)	0.24 (0.02)	3.27 (0.12)	0.09 (0.01)	0.11 (0.02)	1.70 (0.04)	3.73 (0.23)	2.64 (0.07)	0.04 (0.01)	0.37 (0.66)	76
			Aug. 26, 2014	75.62 (0.47)	12.20 (0.10)	0.26 (0.02)	3.27 (0.12)	0.09 (0.01)	0.10 (0.02)	1.70 (0.04)	3.73 (0.38)	2.64 (0.06)	0.04 (0.01)	0.34 (0.46)	*75*
			Sept. 12, 2014	75.63 (0.38)	12.20 (0.09)	0.26 (0.02)	3.27 (0.09)	0.10 (0.01)	0.11 (0.02)	1.70 (0.05)	3.73 (0.37)	2.64 (0.06)	0.04 (0.01)	0.32 (0.38)	*69*
			May 8, 2015	75.57 (0.34)	12.21 (0.09)	0.26 (0.02)	3.29 (0.12)	0.10 (0.01)	0.11 (0.02)	1.72 (0.03)	3.73 (0.31)	2.64 (0.06)	0.04 (0.01)	0.34 (0.52)	*119*
			Sept. 17, 2015	75.57 (0.26)	12.20 (0.09)	0.26 (0.02)	3.27 (0.12)	0.10 (0.01)	0.11 (0.02)	1.70 (0.03)	3.73 (0.22)	2.64 (0.06)	0.04 (0.01)	0.38 (0.38)	*114*
			Oct 1, 2015	75.58 (0.33)	12.20 (0.11)	0.26 (0.01)	3.27 (0.09)	0.10 (0.01)	0.10 (0.01)	1.70 (0.02)	3.73 (0.28)	2.64 (0.06)	0.04 (0.01)	0.37 (0.56)	*32*
			Oct 31, 2015	75.57 (0.23)	12.20 (0.09)	0.26 (0.04)	3.27 (0.32)	0.10 (0.02)	0.10 (0.04)	1.70 (0.02)	3.73 (0.21)	2.64 (0.06)	0.04 (0.01)	0.33 (0.43)	*79*
			May 6, 2016	75.64 (0.60)	12.20 (0.15)	0.26 (0.06)	3.27 (0.39)	0.10 (0.06)	0.10 (0.05)	1.70 (0.05)	3.75 (0.52)	2.64 (0.08)	0.03 (0.01)	0.31 (0.85)	*34*

All major element determinations were made on a JEOL Superprobe (JXA-8230) housed at Victoria University of Wellington, using the ZAF correction method. Analyses were performed using an accelerating voltage of 15 kV under a static electron beam operating at 8 nA. The electron beam was defocused between 10 and 20 μm (except subsidiary VCha Dome banded lava float sample where a 50 μm diameter beam was used). Oxide values are recalculated to 100% on a volatile-free basis. Total Fe expressed as FeO_t. Mean and ±1 standard deviation (in parentheses) based on *n* analyses. All samples normalised against glass standards ATHO-G & VG-568. [1]Chaiten samples (*unpublished data*) retrieved from 17 proximal & distal localities collected by G. Villarosa, V. Outes and B.V Alloway. [#] Analysed by I. Schipper. All other analyses conducted by B.V. Alloway. All individual analyses are available upon request to the corresponding author (BVA).

reconciling these records with vastly different preservational attributes as well as their location within different sectors experiencing ash fall of variable magnitude and/or axes of distribution. To this end, associated stratigraphy, radiocarbon chronology and tephra geochemistry all become particularly important tools for identifying a particular event and establishing correlation with tephra within the soil-forming environment.

2.3. Lower set of VCha-sourced tephra (pre-11,000 and post-18,000 cal a BP)

Tephra layers predating Amarillo Ignimbrite/Lepué Tephra

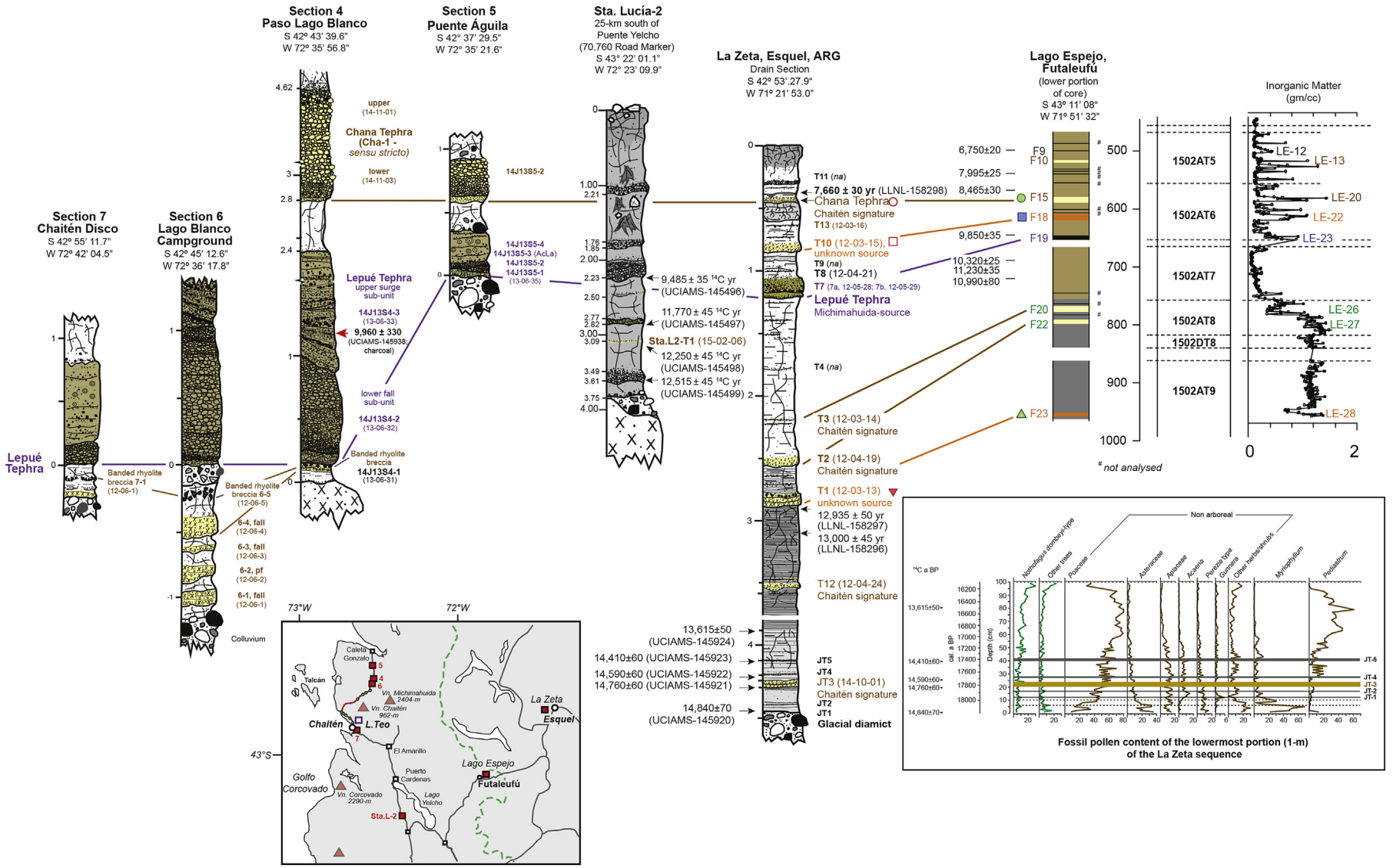

Fig. 8. Stratigraphic columns showing the correlation of the lower set of VCha-sourced tephra (pre-11,000 and post-18,000 cal a BP) from Sections 7, 6, 4 and 5 in the proximal to medial vicinities of VCha, Sta. Lucia-2 located south of VCha, La Zeta drain section located close to Esquel (east of VCha) and Lago Espejo located directly adjacent to Futaleufú ~72 km south-east of VCha. Subfossil pollen content of the lowermost portion (1-m) of the La Zeta sequence is presented as an inset. Brown line designation indicates VCha-sourced tephra of 'old' magma type. Purple line designation indicates the 11,000 cal a BP Lepué Tephra (Alloway et al., 2017). Orange colour designation indicates tephra of rhyolitic composition but of unknown source. Colour-coded numeric designations for tephra section descriptions (and sample numbers) along with the position of radiocarbon dates (presented as ^{14}C a BP) are also indicated. (For interpretation of the references to colour in this figure legend, the reader is referred to the web version of this article.)

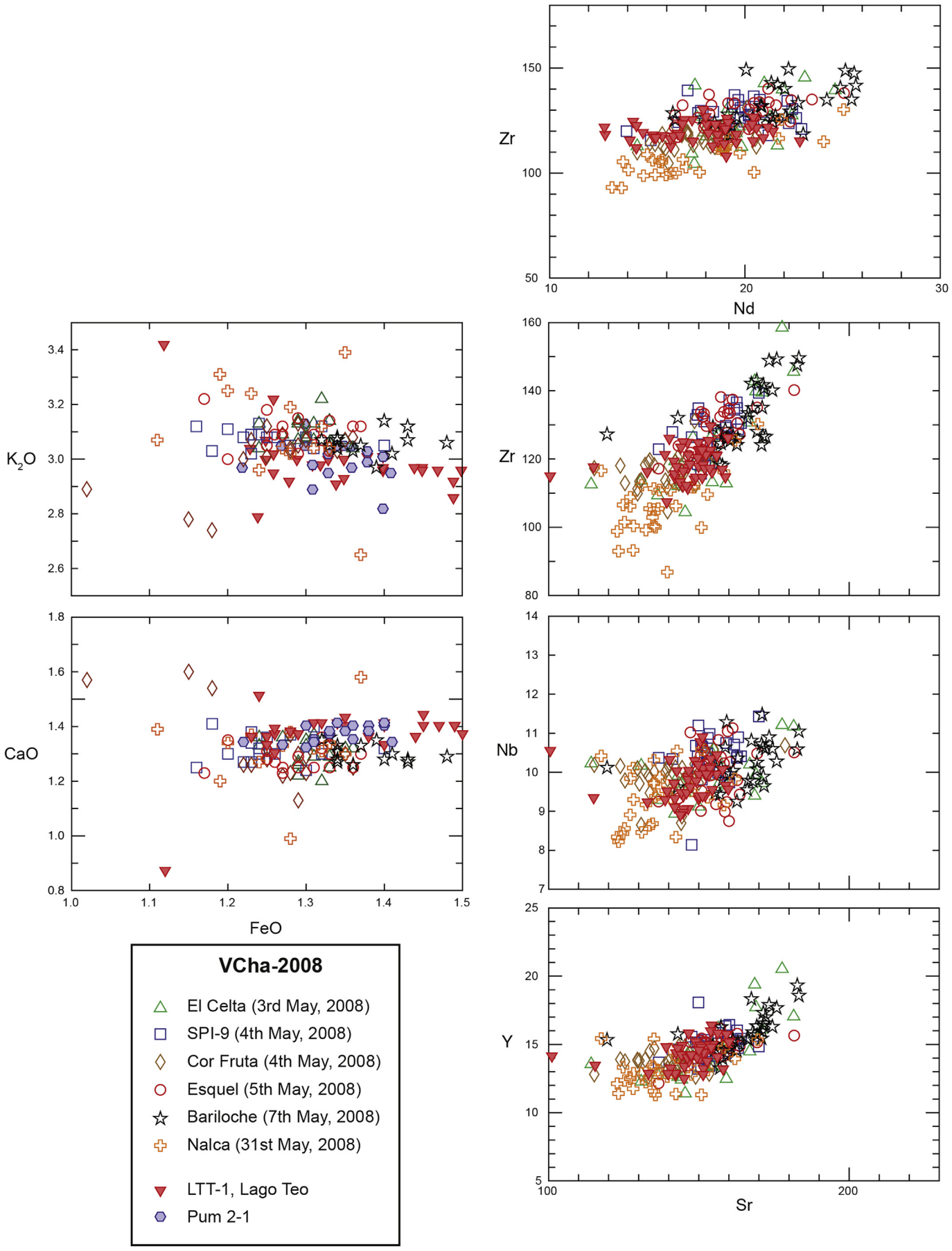

Fig. 9. Selected major (weight percent FeO *vs* K_2O and CaO, normalised to an anhydrous basis) and trace (Sr *vs* Y, Nb, Zr and Nd *vs* Zr) element compositions of freshly deposited glass shards from the VCha-2008 eruption collected from distal sites in Argentina between May 3rd and 31st of that year. EMP and LA-ICP-MS analyses were conducted at the same time and under the same operating conditions. Results indicate subtle compositional domains within the overall elemental field that can be ascribed to different eruptive phases. LTT-1 (VCha-2008) sampled from Lago Teo is tightly clustered but the distribution of major- and trace-element data-points are not compositionally representative of the eruption in its entirety.

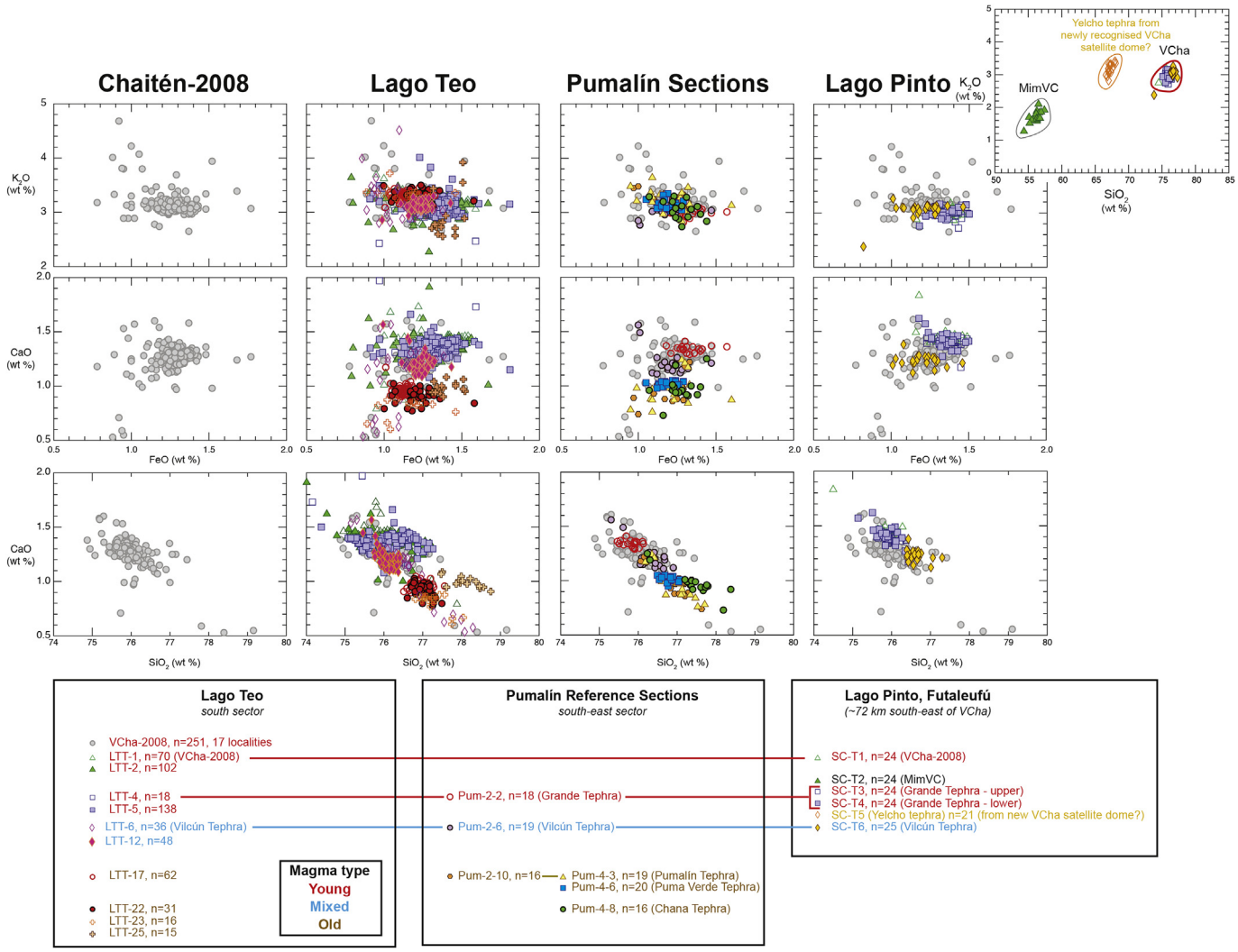

Fig. 10. Selected major-element compositions (normalised to an anhydrous basis weight percent SiO_2 *vs* CaO and FeO *vs* K_2O and CaO) of glass shards from young and middle set of VCha-sourced tephra from Lago Teo, Pumalín Reference Sections 2 and 4, and Lago Pinto located near Futaleufú. Equivalent VCha-2008 elemental data (in grey) are plotted for comparative purposes. Samples are colour coded to reflect subtly different magmatic compositions (red – 'young'; blue – 'mixed'; brown – 'old'). For Lago Pinto all tephra represented are plotted to show that all VCha-sourced tephra are tightly clustered can be easily discriminated from tephra erupted from other sources - in this case - from MimVC (SC-T2) and a newly recognised satellite dome complex located adjacent VCha (SC-T5) (see Discussion). (For interpretation of the references to colour in this figure legend, the reader is referred to the web version of this article.)

(sourced from Volcán Michimahuida at *c.* 11,000 cal a BP; Amigo et al., 2013; Alloway et al., 2017) are uncommon in sectors directly adjacent VCha. At many sections, Lepué Tephra can be observed closely overlying glacio-fluvial sands and glacial diamict (till) draping bedrock and it is consequently useful for determining the rate and timing of deglaciation in this region as the climate ameliorated during the transition between the Last Glacial Maximum (LGM) and early Holocene (Alloway et al., 2017). Rarely, the stratigraphy beneath Lepué Tephra is exposed and a distinctive layer of banded rhyolite breccia and rhyolitic tephra can be observed (Sections 4 and 7; Fig. 8). At a road-side section at Campground Lago Blanco (S6) the basal contact of Lepué Tephra can be clearly observed and is underlain by heterolithologic colluvium, a prominent layer of banded rhyolitic breccia and a sequence of four centimetre-thick rhyolitic ash layers overlying glacial till (Fig. 8). Only within eastern Cordilleran lake sequences (i.e. Lago Espejo and Lago La Zeta; Fig. 8) can older VCha-sourced tephra be recognised.

The paucity of pre-11,000 cal a BP VCha-sourced tephra preserved in the Chaitén sector appears to be a combination of burial by Lepué Tephra or erosion of cover-beds by piedmont glaciation, or both. Much of the Chaitén sector was extensively occupied by ice as recently as *c.* 16,700 cal a BP (*c.* 13,830 ± 50 ^{14}C a BP) (Moreno et al., 2015a; Alloway et al., 2017). In eastern (downwind) Cordilleran sectors, older lake sequences exist that preserve multi-source tephra extending back *c.* 18,000 cal a BP (*c.* 14,800 ^{14}C a BP). At Lago Espejo (Fig. 3) three rhyolitic tephra (two VCha-sourced) can be observed in sediments below Lepué Tephra, whereas at La Zeta 85 km east of Chaitén (Fig. 8) five rhyolitic tephra (four VCha-sourced) intervene between Lepué Tephra above and glacial diamict at the base of the section. A basal age of *c.* 18,000 cal a BP (*c.* 14,800 ^{14}C a BP) effectively extends the eruptive history of an ancestral VCha to the end of the LGM. VCha-tephra (middle and lower sets) have also been documented within sediment cores from Lago Mosquito and Laguna del Cóndor located ~108 and ~125 km north east of VCha, respectively (Iglesias et al., 2012).

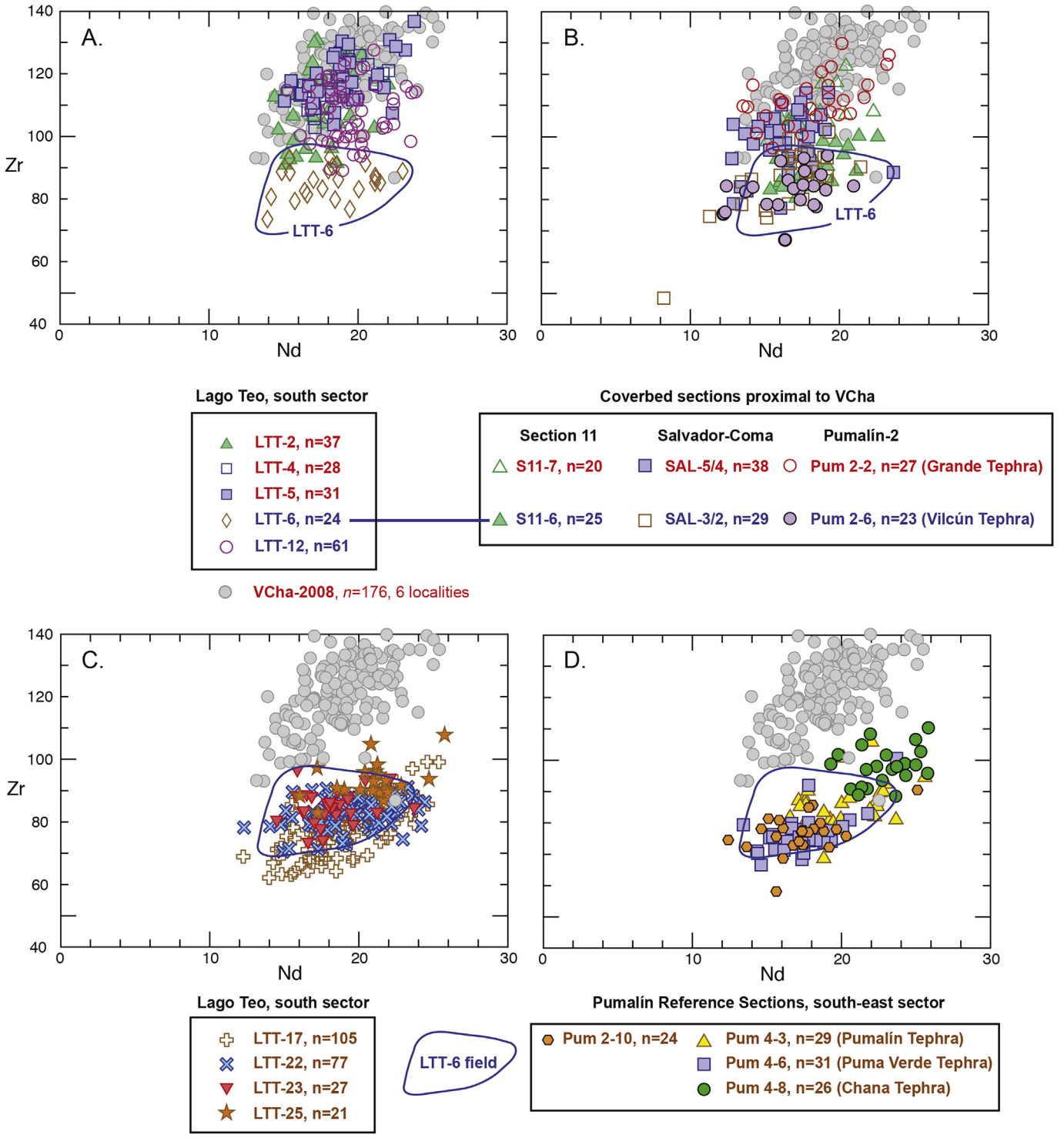

Fig. 11. Nd *vs* Zr composition of glass shards from selected rhyolitic tephra retrieved from Lago Teo as determined by LA-ICP-MS analysis compared with equivalent-aged correlatives from the andic soil-forming environment. Red, blue and brown colour coding indicates VCha-sourced tephra of 'young', 'mixed' and 'old' magma type, respectively. Equivalent VCha-2008 elemental data (in grey) are plotted for comparative purposes. While LTT-6 of mixed magma type can be geochemically distinguished from tephras (LTT-5, LTT-4 and LTT-2) of young magma type, individual units of the young type erupted over the last 600 years cannot be differentiated, including the products of the VCha-2008 eruption (LTT-1). (For interpretation of the references to colour in this figure legend, the reader is referred to the web version of this article.)

3. Palynology of La Zeta section

We analysed the subfossil pollen content of the lower portion of La Zeta sediments (see Fig. 8) to document the paleovegetation and environmental conditions at the very beginning of the last glacial termination (16,000–18,000 cal a BP) - the timing of which is coincident with the deposition of the earliest recognised tephra (both VCha and MimVC-sourced) at this latitude. The record suggests a virtually treeless landscape (arboreal pollen <20%) dominated by grasses (*Poaceae*), shrubs and herbs between 17,100 and

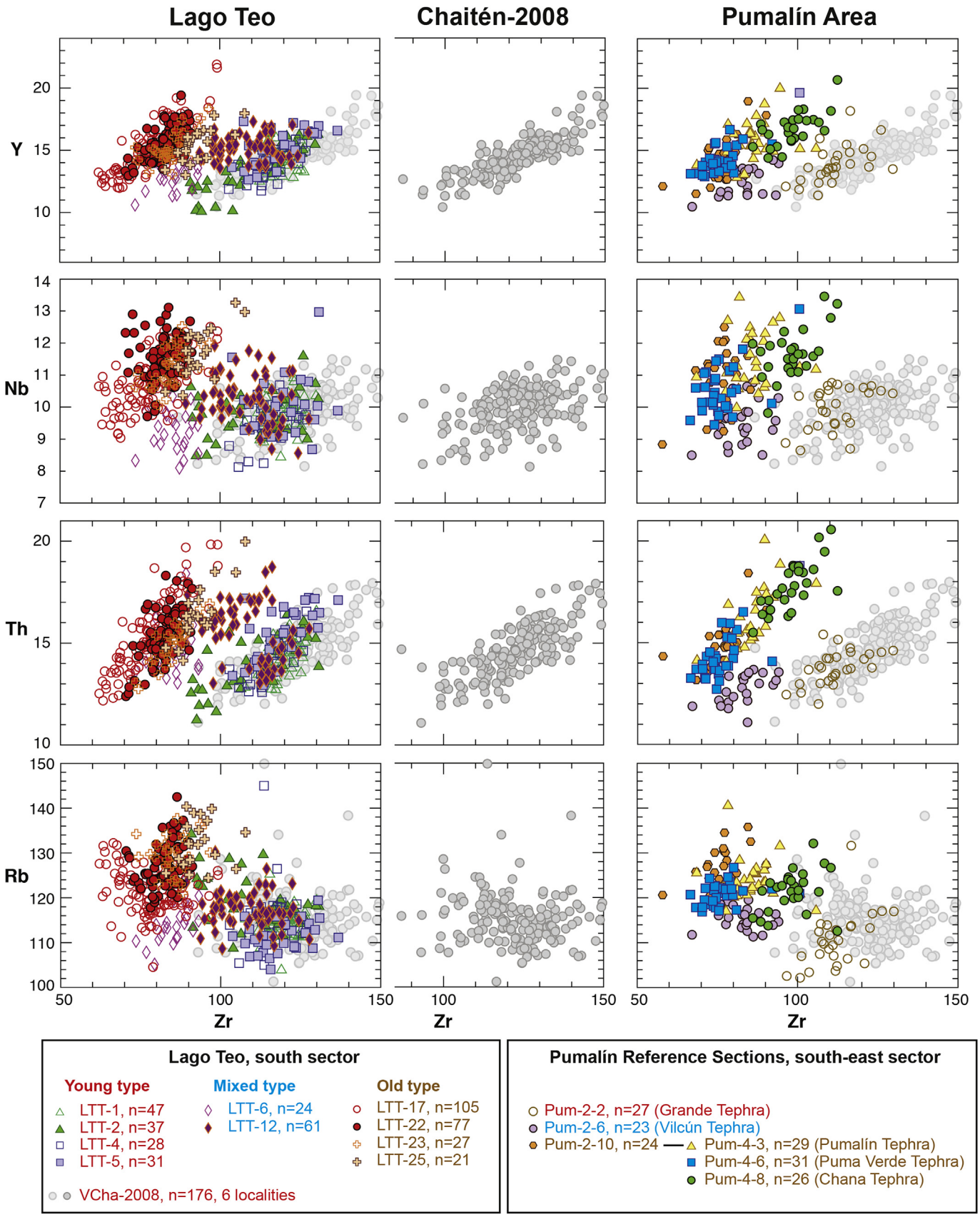

Fig. 12. Zr *vs* Rb, Th, Nb and Y composition of glass shards from rhyolitic tephra retrieved from Lago Teo as determined by LA-ICP-MS analysis compared with equivalent-aged correlatives from Pumalín reference sections. Red, blue and brown colour coding indicates VCha-sourced tephra of young, mixed and old magma type, respectively. Equivalent VCha-2008 elemental data (in grey) are plotted for comparative purposes. Trace element data clearly supports the occurrence of the young, mixed and old magma types as identified from glass shard major-element data. (For interpretation of the references to colour in this figure legend, the reader is referred to the web version of this article.)

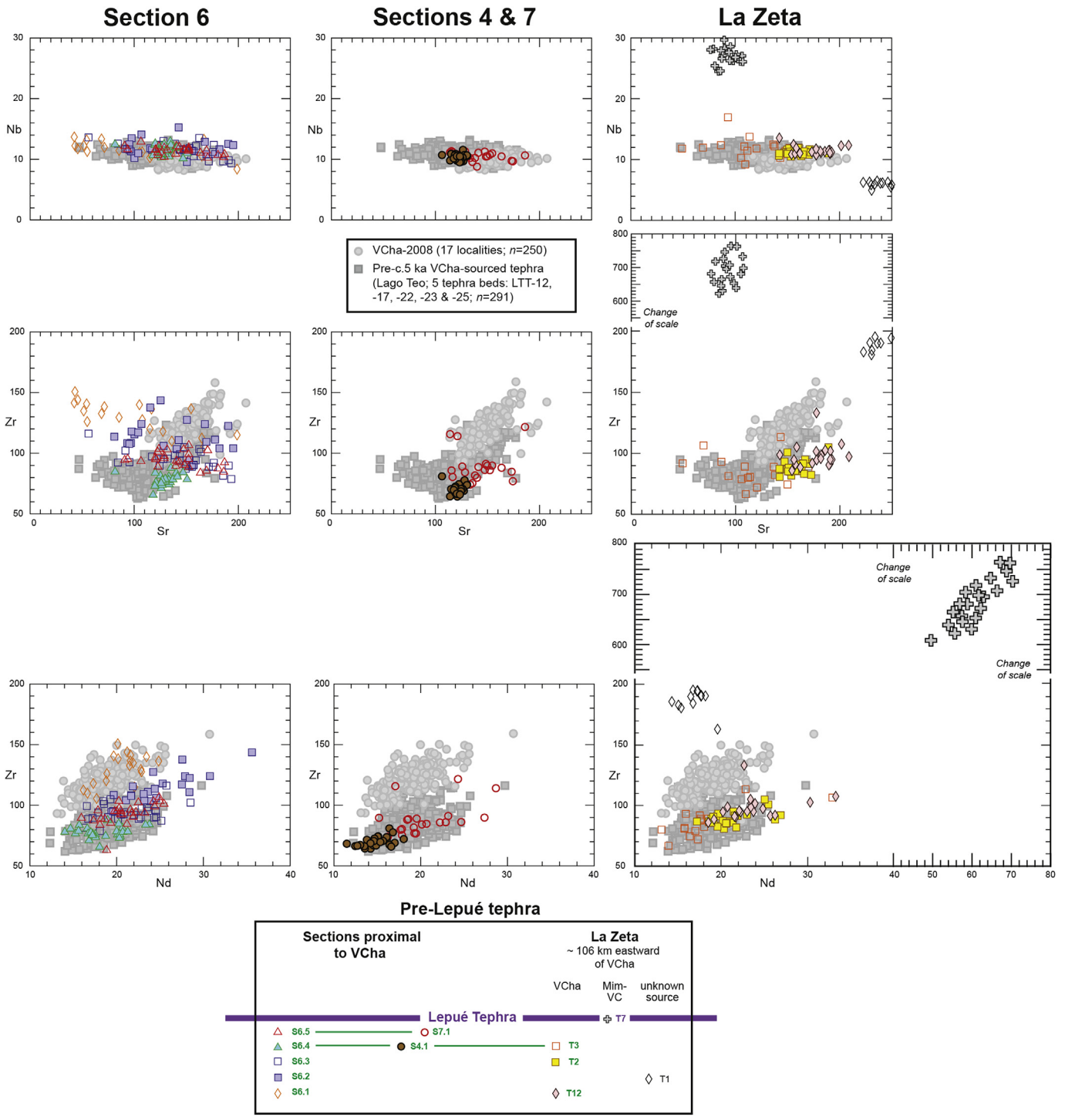

Fig. 13. Selected trace (Nd *vs* Zr and Sr *vs* Zr and Nb) element compositions of pre-11,000 cal a BP rhyolitic tephra of presumed VCha-source from sections proximal to VCha (S4, S6 and S7) and distally at La Zeta, Argentina (~106 km east of source). Equivalent elemental data from VCha-2008 and pre-5000 cal a BP VCha-sourced tephra from Lago Teo are plotted (in grey) for comparative purposes (refer to SI Table 4 for individual elemental analyses). These data confirms a VCha-source for these pre-11,000 cal a BP tephra and indicates their derivation from the old magma type which persisted between *c.* 5000 and *c.* 18,000 cal a BP. Before then, the eruptive record is apparently all but obscured by pervasive Andean piedmont glaciation.

18,000 cal a BP, along with the submerged macrophyte *Myriophyllum*. These results suggest that a pioneer herbaceous community established shortly after local ice recession, with taxa commonly found in alpine environments and the Patagonian Steppe along with littoral species indicative of shallow lake levels. VCha tephra (JT3) and MimVC tephras (JT1, -2, -4 and -5) were deposited during this interval. The record then shows a rise in Poaceae and the planktonic alga *Pediastrum*, and a slight increase in arboreal pollen between 16,000 and 17,100 cal a BP suggesting either an increase in precipitation or higher effective moisture.

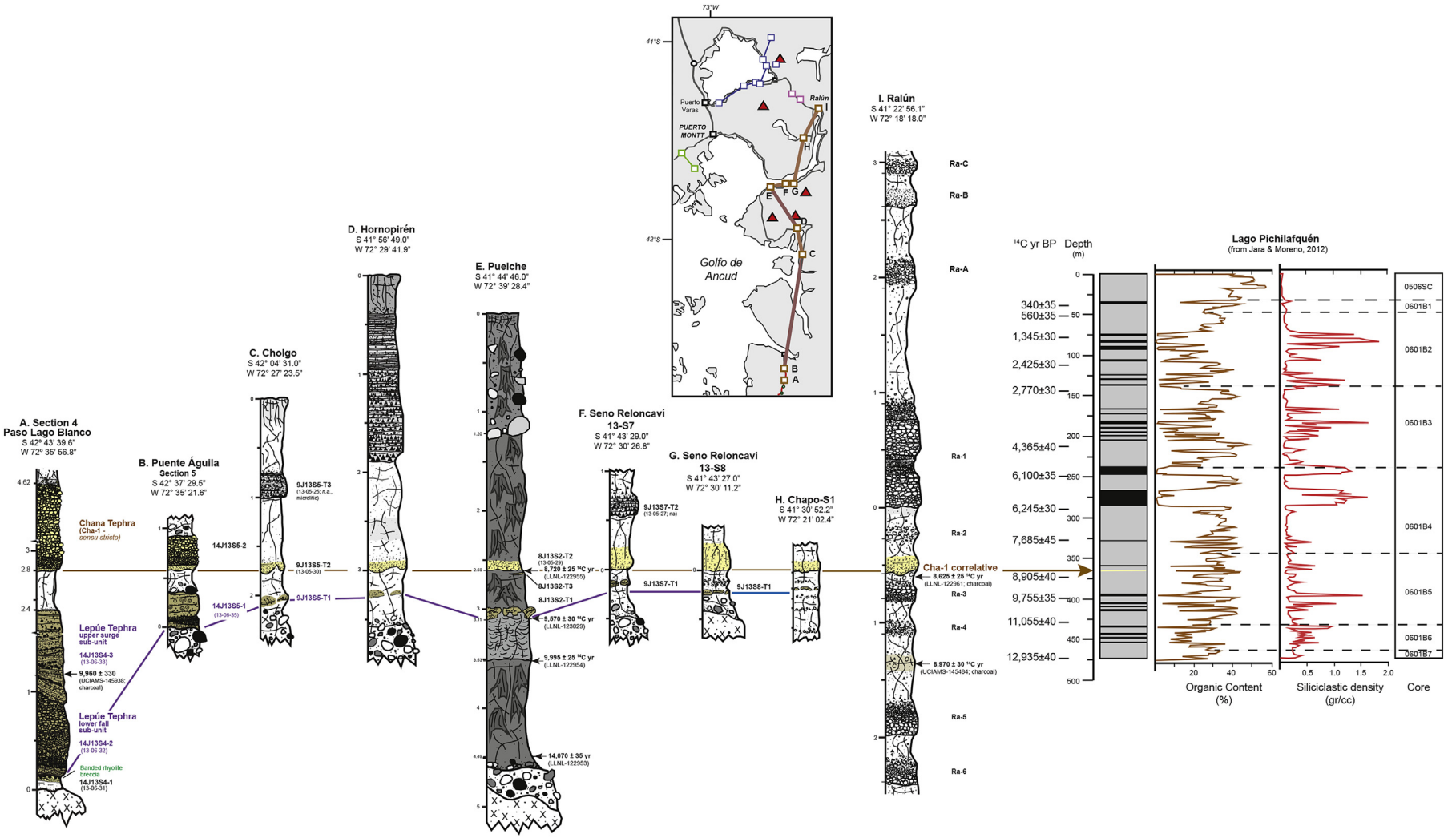

Fig. 14. Stratigraphic columns showing the correlation of Cha-1 from Section 4 Paso Lago Blanco northwards to Ralún at the head of Seno Reloncaví. Cha-1 can be correlated further north where it occurs as an 8-mm thick layer within sediment cores from Lago Pichilafquén (Jara and Moreno, 2012) located close to Lago Puyehue. Note the persistent occurrence of the 11,000 cal a BP Lepué Tephra closely underlying Cha-1 at most localities. The positions of radiocarbon dates (presented as ^{14}C a BP) are also indicated.

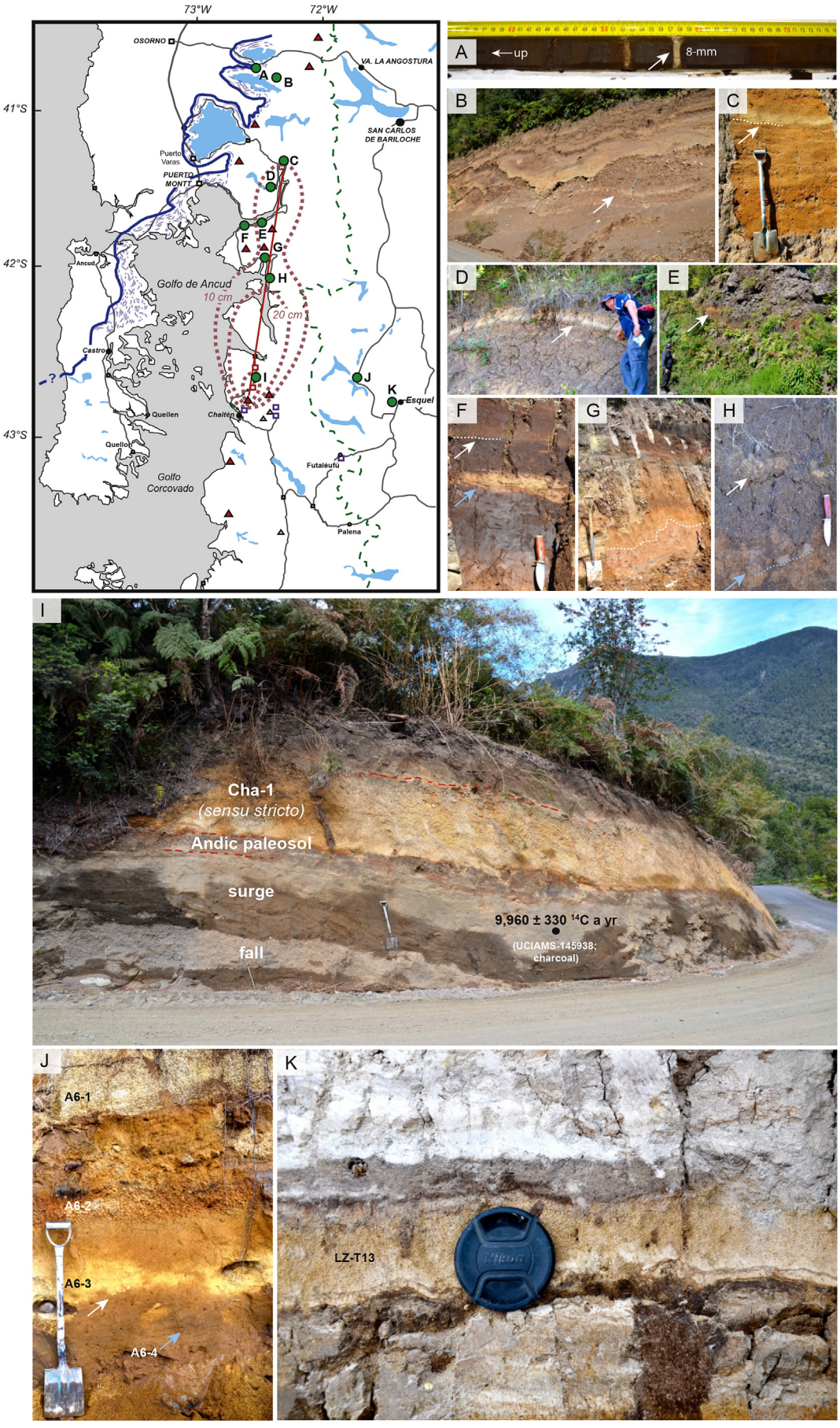

Fig. 15. Chana Tephra (Cha-1) expressed within lake sediments and cover bed sections of north-western Patagonia. White arrow indicate the position of Cha-1, while blue arrow indicates the underlying occurrence of Lepué Tephra (Alloway et al., 2017) **A.** 8-mm thick bed at ~3.70-m depth within sediment cores retrieved from Lago Pichilafquén (Jara and Moreno, 2012); **B**. Antillanca; **C**. Ralún; **D.** Lago Chapo; **E.** Seno Reloncaví; **F.** Puelche; **G.** Hornopirén; **H.** Cholgo; **I.** Paso Lago Blanco; **J.** Parque Alerce, Argentina and **K.** La Zeta, Argentina. The inset map shows the distribution of these descriptive sites with respect to the Cha-1 isopach map produced by Watt et al. (2015). (For interpretation of the references to colour in this figure legend, the reader is referred to the web version of this article.)

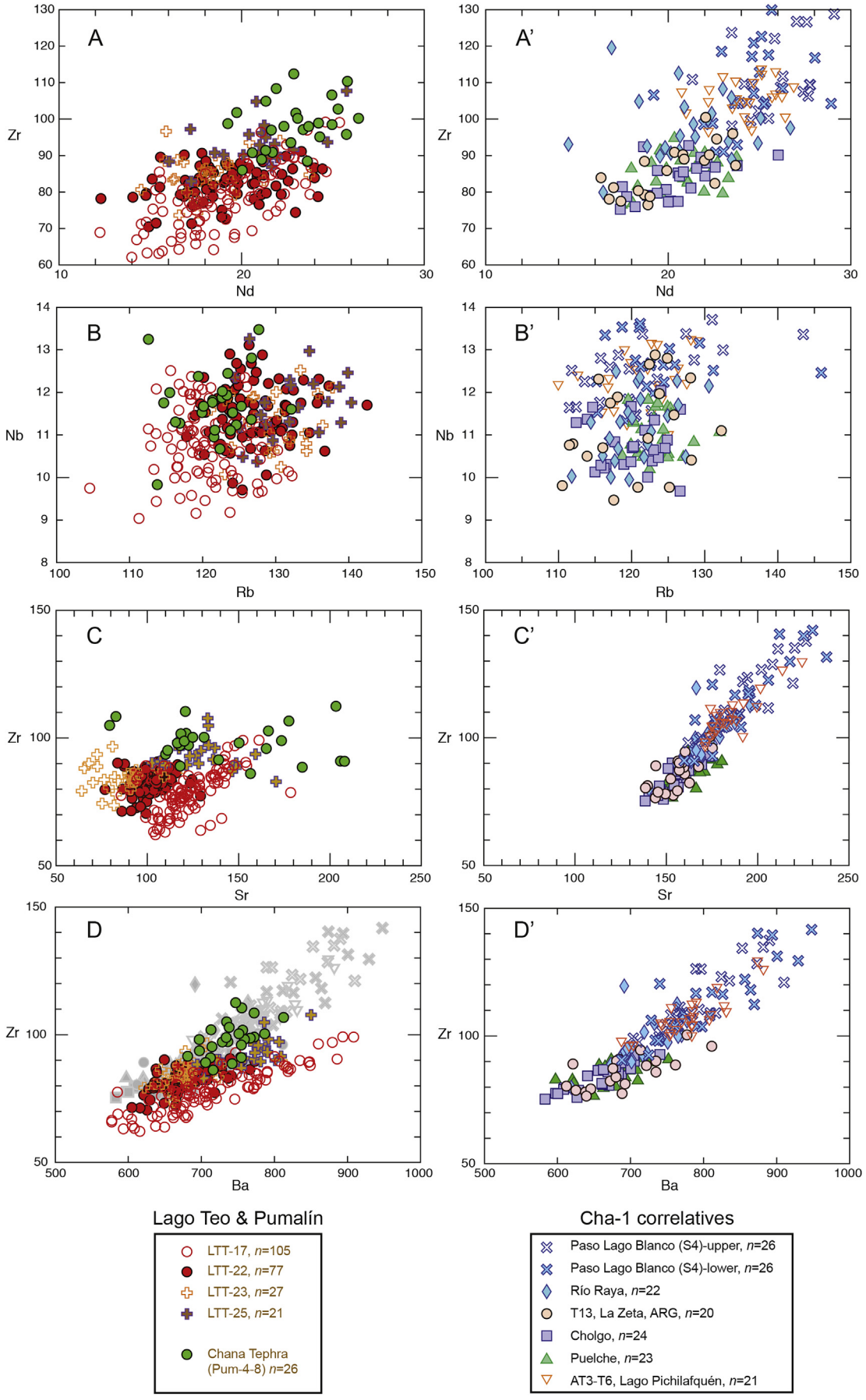

Fig. 16. Selected compatible and incompatible trace element data (Zr *vs* Nd, Nb *vs* Rb; Zr *vs* Sr and Ba) for tephra deposits from Lago Teo (LTT-17, -22, -23 and -25) and Chana Tephra from Pumalín-4 (A-D) compared against Cha-1 correlatives (A′-D′) from proximal S4, Raya and distal (La Zeta, Cholgo, Puelche and Pichlafquén) occurrences. Note the similarity in incompatible element ratios for all samples, but that differences in magma compositions are apparent in terms of their compatible element compositions (Ba, Sr). Note how Chana Tephra has compositions of both the high and low Sr groupings, linking the LTT record with Cha-1.

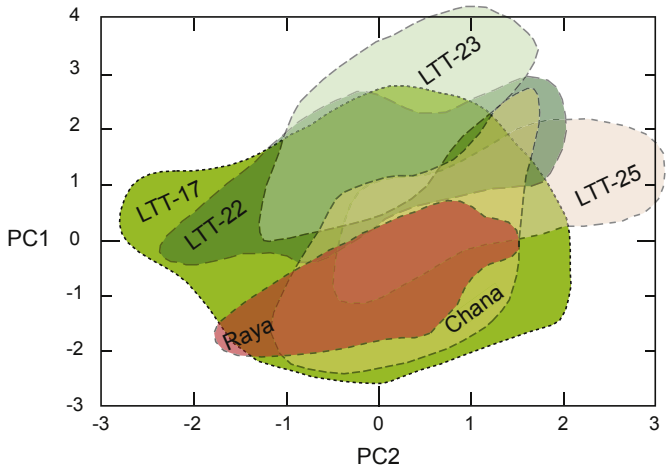

Fig. 17. Principal component analysis (performed using a correlation matrix in Minitab v. 14) using Rb, Sr, Cs and Ba which shows the compositional overlap between Raya (Cha-1 correlative), Chana Tephra and the lowermost Lago Teo sample LTT-25. Note how these PCA fields differ from LTT-22 and LTT-23, and the larger field occupied by LTT-17.

4. Geochemistry

We report major- and trace-element chemistries of pumice and glass from trachyte-dacite-rhyolite tephra determined from grain-discrete EMP and LA-ICP-MS analyses (see Table 2; SI Tables 1–6). We use these data to affirm source, discriminate between tephra sourced from the same and adjacent centres, as well as provide some insights into the composition and temporal evolution of clustered magma occurring in the sub-volcanic system beneath VCha.

The most recently erupted VCha-tephra was collected at distal Argentine localities in time series from the commencement of the eruption on May 3rd to 31st May 2008 (Fig. 9; SI Tables 1 and 2) and provides an important analytical template with which other VCha-sourced tephra can be compared. Overall, the composition of the VCha-2008 ash is relatively uniform. Both major- and trace-element compositions of glass shards analysed from downwind Argentine locations during different eruptive phases indicate subtle compositional domains within the overall elemental field and appear to represent a time series spanning different compositions. This finding supports the conclusion of Watt et al. (2009) who also recognised discrete domains within the overall compositional range occupied by samples from specific depositional lobes. It is interesting to note that LTT-1 (VCha-2008) sampled from Lago Teo is tightly clustered but the distribution of major- and trace-element points is not compositionally representative of the eruption in its entirety. This aspect has implications when attempting to correlate the same tephra but in different sectors (and were presumably deposited during different eruptive phases at different azimuths) or different aged tephra erupted from the same point source. Consequently a cautious interpretive approach to correlation is required, at least until a spatially wider (and more representative) set of analyses can be acquired or correlation based on a small spatial spread of analyses can be additionally supported by a combination of identifiable field characteristics (i.e. bedding architecture), chronology and stratigraphic association (Shane et al., 2007; Lowe and Alloway, 2015).

The major-element data for all rhyolitic tephra from Lago Teo is already documented (Moreno et al., 2015b). This data indicates that LTT-2, -4 and -5 are indistinguishable in major-element glass chemistry from LTT-1 (VCha-2008) with LTT-6 having a slightly different (though related) glass composition compared with the set of closely overlying VCha tephra. Correspondence of major-element data between rhyolitic tephra occurring within Lago Teo in the south sector, Pumalín reference sections in the south-east and Lago Pinto, Futaleufú ~72 km south east of VCha, is shown in Fig. 10 (see also SI Table 3). Vilcún Tephra (i.e. Pum-2-6 and SC-T6) has indistinguishable major-element glass chemistry from LTT-6 (*c.* 850 cal. a BP) and the considerably older LTT-12 (*c.* 5078 cal. a BP) but quite different trace-element glass chemistries (e.g. see Fig. 11A).

These same elemental groupings are supported by trace element data (this study; see SI Table 4) and can be clearly seen in Nd *vs* Zr (Fig. 11) and the Zr *vs* Rb, Th, Nb and Y (Fig. 12) bivariate plots. LTT-6 is indistinguishable from Vilcún Tephra (i.e. S11-6, pSC-2/3 and Pum-2-T6), while LTT-2, -4 or -5 cannot be chemically differentiated from Grande Tephra (i.e. S11-7, pSC-4/5 and Pum-2-2) which closely overlies Vilcún Tephra in sections proximal to VCha (see Figs. 2, 3 and 5). Similarly, members of the middle rhyolitic tephra set from Pumalín cover-bed sections (i.e. Pumalín, Puma Verde and Chana Tephras; see Figs. 4 and 6) cannot be differentiated from older tephra occurring within Lago Teo (LTT-17, -22, -23 and -25). Although middle and younger tephra sets can be distinguished from each other, discrimination of individual members within each tephra set cannot be solely resolved by major and/or trace glass chemistry - chronological equivalence is an important consideration in effective correlation. Nevertheless, major- and trace-element glass shard data from both the Lago Teo core and soil cover-bed sections are for the most part coincident (Fig. 12) and support the occurrence of 'Young', 'Mixed' and 'Old' magma batches.

Trace element data of rhyolitic tephra pre-dating Lepué Tephra (*c.* 11,000 cal a BP) are presented in Fig. 13 (see also SI Table 4). Zr *vs* Nd and Sr *vs* Zr and Nb bivariate plots clearly indicate these rhyolitic tephra from Sections 4, 7 and 6 located in the vicinity of Chaitén (see Fig. 1) and those exposed at La Zeta, ~106 km east of VCha, all have a VCha chemical signature and are indistinguishable in chemistry from pre-5 cal. ka VCha-tephra but at La Zeta the VCha tephra can be chemically differentiated from Lepué Tephra (LAZ-T7) sourced from Mim-VC (Alloway et al., 2017) and a rhyolite tephra from an unknown source (i.e. LAZ-T1). It is feasible that LAZ-T1 (and potentially LAZ-DI) has similar Zr/Th, Zr/Ce, Zr/Hf, Zr/U ratios to Lepue Tephra and therefore might represent lesser evolved rhyolitic eruptives similarly sourced from MimVC. Of the pre-11,000 cal a BP VCha-sourced tephra, only the lowermost tephra at Section 6 (S6.1) is sufficiently different in chemistry (i.e. Zr/Th ratio) from those closely overlying it to be identifiable at other sites (see SI Table 4). Unfortunately, no other occurrences of this tephra are known at this stage and this same tephra does not appear to be represented eastward within paleolake sediments of the La Zeta section.

5. Discussion

5.1. Three magma types

Zr/Nd and Zr/Th ratios define at least three discrete but closely related magma compositions. The older cluster, with Zr/Nd $\leq$ 5.4 and Zr/Th $\leq$ 6.5 comprise LTT-25, -23, -22 and -17 at Lago Teo and Pumalín, Puma Verde and Chana Tephra from the andic soil forming environment. The younger cluster with Zr/Nd $\geq$ 5.4 and Zr/Th $\geq$ 6.5 comprise LTT-5, -4, -2 and -1 at Lago Teo and Grande and VCha-2008 tephras. LTT-12 and -6 from Lago Teo and Vilcún Tephra from the soil-forming environment appear to be a mixture of both old and young magma types. LTT-6 is *c.* 851 cal. a BP and while its major-element glass chemistry is compositionally similar to LTT-12,

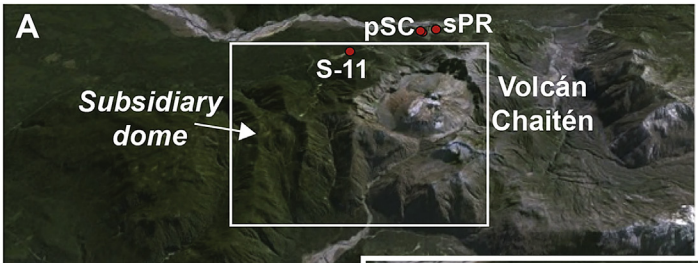

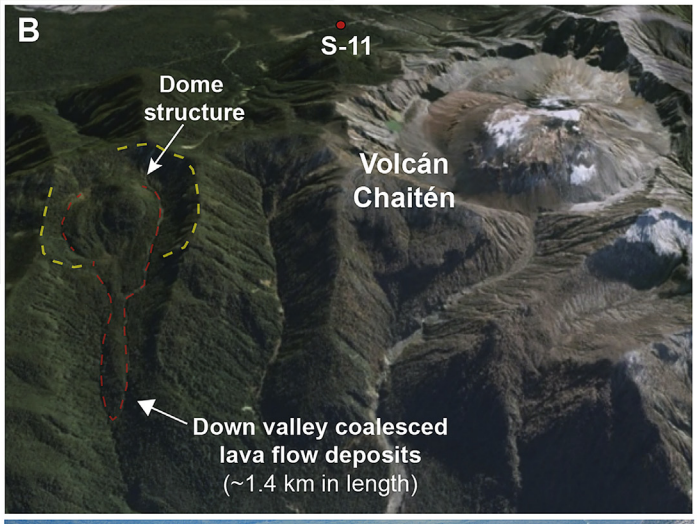

Pumalín-2
S 42° 55' 23.0"
W 72° 23' 56.0"

Lago Pinto, Futaleufú
(~72 km south-east of Volcán Chaitén)
S 43° 09' 27.4"
W 71° 54' 07.6"

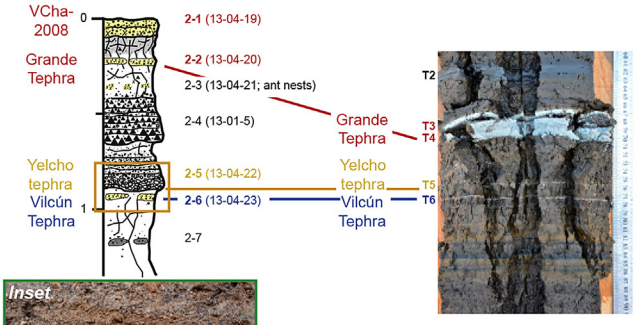

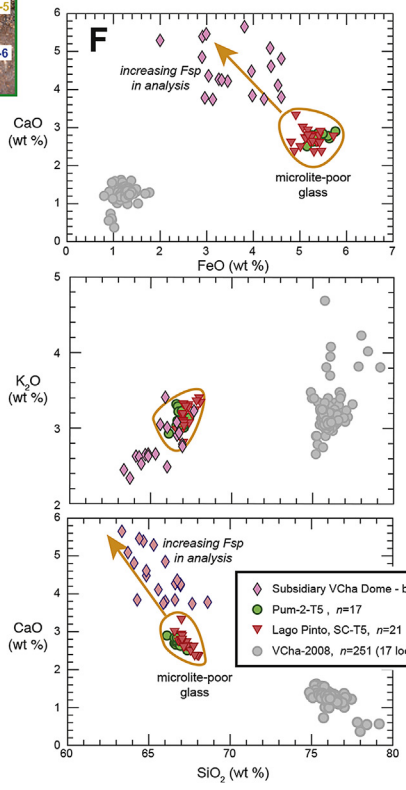

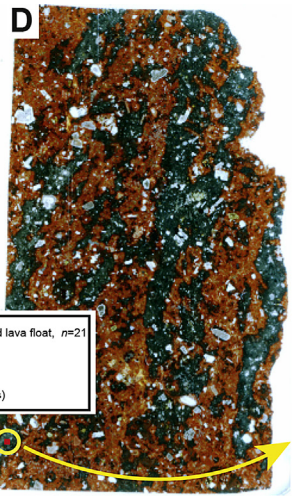

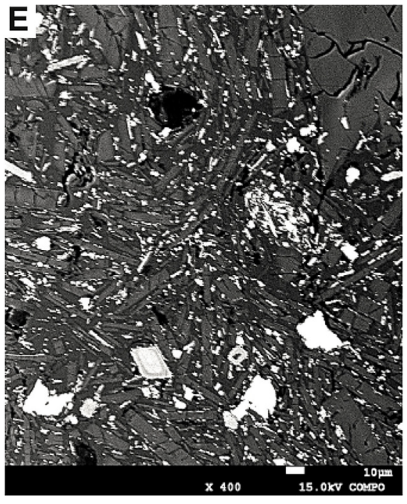

the product of a significantly larger eruption that took place at *c.* 5078 cal. a BP, its selected trace-element composition is quite different and indistinguishable from post-Vilcún VCha-eruptives (e.g. VCha-2008, LTT-2, -4 and -5; Fig. 11). However, the correlation of LTT-12 from Lago Teo in the south sector to the soil cover-bed sequences located in the south-east remains problematical in that a rhyolitic tephra of comparable chemistry to LTT-12 has yet to be identified though it clearly has a similar age to Pumalín Tephra (constrained by bracketing ages of *c.* 4756 and *c.* 5523 cal. a BP from Lago Espejo, Futaleufú and a maximum age of *c.* 5408 cal. a BP from Alerce-6; see Fig. 4).

5.2. Correlation of Cha-1 sensu stricto

Cha-1 (*sensu stricto*) was originally described and defined by Naranjo and Stern (2004) in the immediate vicinity of Section 4 (S-4, Paso Lago Blanco). At this locality Cha-1 closely overlies fall and surge sub-units of Lepué Tephra (Alloway et al., 2017) (see Fig. 14). In this study, Cha-1 can be correlated northwards from Paso Lago Blanco (S-4) to Ralún at the head of Seno Reloncaví (see Fig. 10) but can also be traced further north to Lago Pichilafquén (Jara and Moreno, 2012) located near Lago Puyehue and within road sections in the vicinity of Antillanca (see Fig. 15A and B). This transect closely coincides with the axis of distribution as described by Watt et al. (2011, 2015) (see map inset in Fig. 15).

Radiocarbon samples collected immediately beneath Cha-1 at Puelche and Ralún (Fig. 10) yielded ages of 9619 ± 47 and 9543 ± 23 cal a BP (Fig. 14; Table 1), respectively and are broadly similar to ages of 9873 ± 157 (SUERC-21502) and 9966 ± 136 (LR0901B T6-50) cal. a BP reported by Watt et al. (2011) and Fontijn et al. (2016), respectively. The difficulty is being able to correlate Cha-1 with one of the three closely spaced centimetre-thick tephra (LTT-25, -24 and 22) at the base of the Lago Teo core. Here, these tephra form discrete, massive to normal-graded ash beds with sharp upper and lower contacts with no obvious evidence of upward redeposition, and consequently, can be considered as successive airfall beds. These three tephra are similar in glass shard major-element chemistry (see SI Table 5) and have modelled median ages of 9678, 9592 and 9462 cal a BP, respectively (Moreno et al., 2015b). The question is which one of these three closely spaced tephra correlates with Cha-1?

In order to be able to locate Cha-1 firmly within the Chaitén tephrostratigraphic framework we compared the trace element chemistry of Cha-1 correlatives from its northward transect to tephra represented in the lower portions of the Lago Teo sediment core (LTT-17, -22, -23 and -25) as well as Chana Tephra (Pum-4-8) from the Pumalín-4 section (Fig. 4; see SI Table 6). Selected trace element bivariate plots for largely incompatible elements (i.e. Zr *vs* Nd and Nb *vs* Rb; Fig. 16A-A′, B-B′) of Lago Teo and Chana Tephra appear indistinguishable from Cha-1 correlatives, and indicate a co-genetic source for these deposits. However these differ when some compatible elements are considered (e.g. Zr *vs* Sr and Ba; Fig. 16C-C′, D-D') where differences in these tephra deposits are apparent, and these plot in two separate compositional groups of magmas.

(i) a lower Sr group which includes LTT-17, 22, 23, 25 and (ii) a generally higher Sr group (150–250 ppm Sr) which includes Chlogo, La Zeta and Puelche at Zr concentrations <100 ppm, and the upper and lower samples from S-4 at Paso Lago Blanco and Pichilefquén at Zr > 100 ppm.

The higher Sr group (ii) displays a linear fractionation trend consistent with the eruption of a zoned magma with ongoing feldspar extraction, and covers a range of compositions similar to that displayed by the VCha-2008 eruption, which vented magma of different compositions, ejected in different directions on different days (Watt et al., 2009) (see Fig. 9). With such a scenario (different portions of a zoned magma chamber and/or chambers being ejected during an eruptive event), and potentially involving more than one co-eruptive point source, a compositionally diverse tephra deposit can result. This may require detailed consideration to allow correlation or discrimination between overlapping but subtly different populations, and if this was the case in the Cha-2008 eruption, it seems likely that similar eruptive scenarios may have operated in the past.

In the case of the Cha-1 tephra correlatives, glass from Chana Tephra straddles the low-Sr (i) and high-Sr (ii) groups, with its high Sr component overlapping with the composition of Raya, which sits in the centre of the array of high-Sr samples with ~100 ppm Zr (see Fig. 16C-C'), the low-Sr glass from the Chana Tephra occupies the same compositional space as LTT-25. The Chana Tephra thus links Raya (and the Cha-1 correlatives) with LTT-25. As the data indicates, the connection is not magmatically straightforward and may result from eruption of different (and/or differently evolved) magma batches being available at the same time. Principal component analysis (PCA, performed using a correlation matrix in Minitab v. 14) using Rb, Sr, Cs and Ba shows the compositional overlap between Raya, Chana and LTT-25, and also the subtle differences existing between those three correlatives to those of subsequently erupted VCha-sourced tephra represented within Lago Teo (i.e. LTT-17, LTT-22 and LTT-23; see Fig. 17). From the PCA, and the chemical data described above, we conclude that the most likely correlation is between Raya, Chana and LTT-25, making LTT-25 the Cha-1 correlative in Lago Teo.

5.3. The occurrence of a newly recognised late Holocene lava dome adjacent to VCha

As VCha-sourced tephra were being mapped, a subsidiary dome nested within the upper tributary of a stream valley occurring less than 2 km south west of the present-VCha was recognised (Fig. 18A-C). Here lava flows can be observed extending ~1.48 km down-valley from the dome and aerial survey indicate at least two effusive vents. This dome is approximately a tenth of the size of the present-day VCha dome (~0.37 km diameter compared with the combined diameter of ~3.10 km for the two coalescing post-2008 domes). Multiple attempts to reach this dome have thus far been unsuccessful, thwarted by a series of very densely vegetated

Fig. 18. Annotated Google Earth images of the newly recognised subsidiary lava dome showing (**A**) its location with respect to VCha and proximity to Lago Teo and Chaitén township, and (**B, C**) dome features interpreted from aerial survey as well as associated flows extending ~1.4 km down-valley. Note the proximity and orientation of the tributary valley containing the dome structure with respect to Chaitén township; **D.** Polished thin section of lava from the newly recognised satellite VCha dome. A backscattered electron (BSE) image is presented in **E** to show a representative area of matrix that is dominated by aligned prismatic plagioclase microphenocrysts with very minor interstitial glass; **F.** Selected major-element compositions (normalised weight percent SiO_2 *vs* K_2O and FeO *vs* CaO and K_2O) of glass from Yelcho tephra (Pum-2-T5 and Lago Pinto SC-T5) compared with analyses from the subsidiary dome float sample. 2008 Chaitén tephra analyses (retrieved from 17 distal localities) are included for comparative purposes and are indicated in grey. EMP analyses from the dome float sample provide a "bulk" modal composition of between 63 and 68 wt % SiO_2 and represents analyses of dominantly feldspar with varying amounts of glass (see Table 2 and SI Table 3). The strong linear relationship of major-elements (i.e. between SiO_2 and CaO) is a reflection of feldspar ablation during analysis with an increase of wt. % CaO at the expense of SiO_2. The highest wt % SiO_2 *vs* K_2O values obtained for this trachyte-dacite float material is similar to equivalent clustered values of glass shard analyses from Yelcho tephra (Pum-2-T5 and Lago Pinto SC-T5; see Fig. 2). Given the coarse lapilli texture of Yelcho tephra (P2-5) at Pumalín-2 and many other sites along the Rio Michimahuida, a nearby eruptive source is likely. The connection between this newly recognised satellite dome and potential co-eruptive products remains to be confirmed.

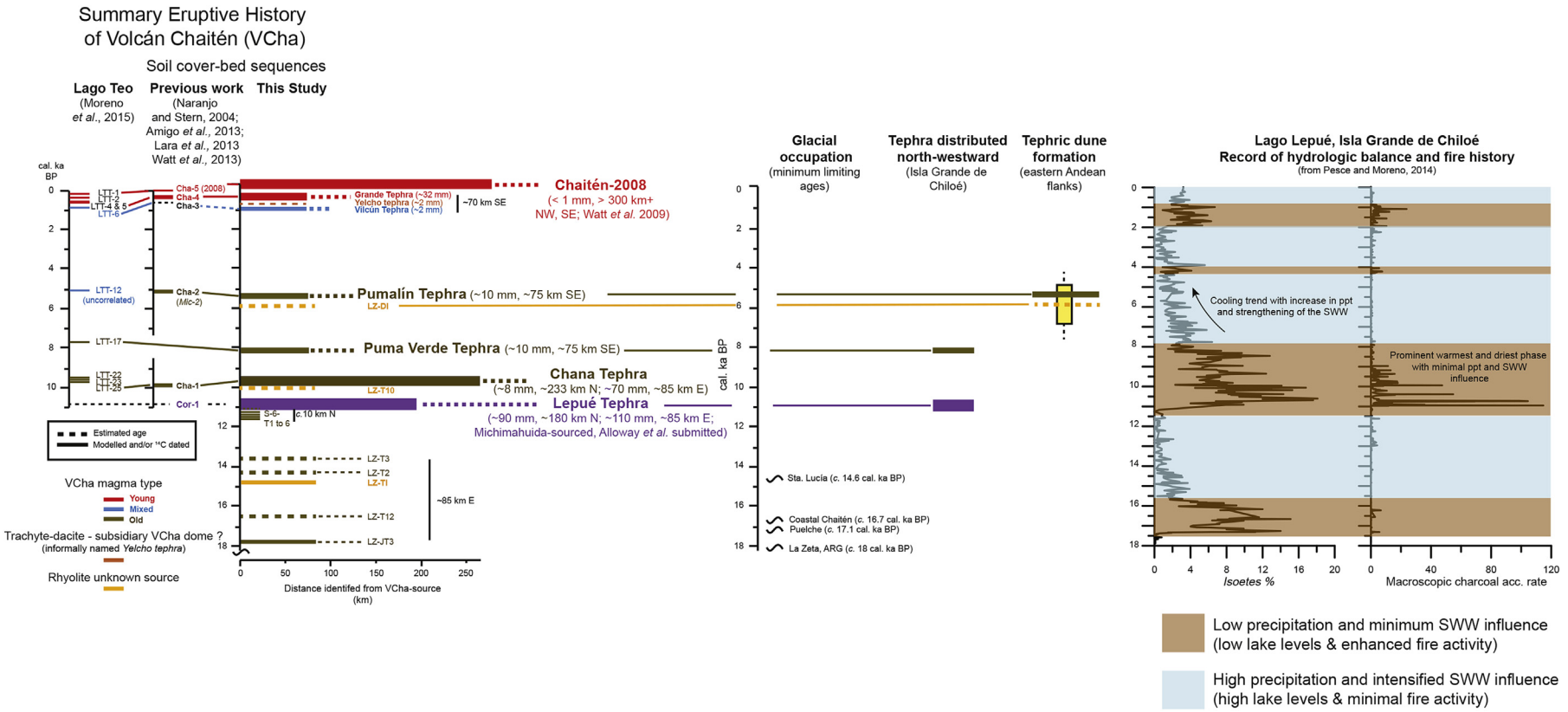

Fig. 19. Summary eruptive history of VCha from present day extending back to *c.* 18,000 cal a BP. Twenty VCha-sourced tephra are recognised. An attempt is made (this study) to place all previous observations (i.e. Naranjo and Stern, 2004; Amigo et al., 2013; Lara et al., 2013; Watt et al., 2013b; Moreno et al., 2015b) firmly within a coherent stratigraphic framework. Cha-designated tephras are renamed in accordance with the International Stratigraphic Code (see Supplementary Information 2.0). VCha-sourced tephra are arranged chronologically with their magnitude differentiated on the basis of their primary thickness/distance from source. Line thickness provides a visual indication of distal prominence of a particular event, while the gradation of solid to dashed horizontal lines indicate the likely occurrence of a tephra beyond its current distal-most point of recognition. Minimum limiting ages for glacial occupation are indicated because glacial positions will likely affect the preservation potential of earlier erupted VCha tephra. An attempt is made to link the distribution and depositional character of VCha-sourced tephra with prevailing climatic conditions at the time of eruption. Tephra distributed north-westwards are noted as are those tephras that form prominent dune fields along the eastern Andean flanks. These fragmentary observations are placed within the context of one of the most complete paleoclimatic records from northwestern Patagonia extending from present-day to the LGM recorded from Lago Lepué located in the central-east Isla Grande de Chiloé (43°S) (Pesce and Moreno, 2014).

bedrock escarpments with large waterfalls and lack of helicopter landing sites. Rock debris (float) within the stream valley, extending directly from the dome and its associated lava flow deposits overwhelmingly comprises metamorphic basement material with subordinate volcaniclastic debris. Aside from the occurrence of columnar jointed fine-grained dyke material, the source of which was located and observed intruding basement within the medial reaches of the stream valley, all remaining volcaniclastic float is of extrusive origin (lava flow material), and is texturally and mineralogically homogenous, suggesting a singular up-valley source, an observation in accord with the aerial survey. Preliminary EMP analyses (see Table 2 and SI Table 3) were undertaken on float samples derived from the newly recognised satellite dome and then directly compared with banded rhyolite from the 2008 dome. The matrix of the subsidiary dome float is entirely occupied by aligned prismatic plagioclase microphenocrysts with subordinate interstitial glass (Fig. 18-D, E). Consequently, EMP analyses provide a "bulk" modal composition of between 63 and 68 wt % SiO_2 and represents analyses of dominantly feldspar with varying amounts of glass. The strong linear relationship of major-elements (i.e. between SiO_2 and CaO; see Fig. 10) is a reflection of incorporation of feldspar during analysis giving an increase of CaO at the expense of SiO_2. The highest SiO_2 concentration obtained for this trachyte-dacite float material is similar to the SiO_2 content of glass shard analyses from a brown centimetre-thick medium to coarse pumiceous lapilli bed (Pum-2-T5) of unknown origin occurring within the south-east sector, where its consistently coarse (lapilli) grain-size suggests a nearby source. This tephra is exposed prominently within sections along road W-887 (i.e. Pumalín-2) and occurs between a scoriaceous basaltic lapilli (Pum-2-T4) above and Vilcún Tephra (Pum-2-T6; *c.* 850 cal. a BP) below. This same trachyte-dacite tephra has been identified within sediments of Lago Pinto, near Futaleufú (~72 km south-east of VCha). On the basis of our preliminary chemistry there remains a strong likelihood that Pum-2-T5 and its distal correlative from Lago Pinto (SC-T6) may originate from this satellite dome. However, the connection between this newly recognised satellite dome and co-eruptive products remains to be definitely proven. If this connection can be confirmed, then the occurrence of this dome effectively broadens the extent of known vents recently involved in past VCha eruptions, and considering the proximity and orientation of the tributary valley containing the dome structure with respect to Chaitén township, represents a previously unforeseen and additional hazard should it ever reactivate. Whatever its relationship to VCha activity, the occurrence of this dome also points to the compositional diversity and tight clustering of magma bodies apparently resident in close proximity within, and directly adjacent to, the sub-volcanic system of VCha.

5.4. Eruptive records and their placement within the context of late Quaternary paleoenvironmental records of NW Patagonia

In recent years with the growing appreciation of the utility of tephra as isochronous horizons by the paleoecological community there has been considerable progress in establishing the link between VCha-sourced tephra occurrence with equivalent-aged vegetation and climate change, fire-regime shifts and volcanic disturbance in Chiloé Continental (43°S) during the last 10,000 years (i.e. Henríquez et al., 2015). As sedimentary records are being steadily resolved in detail and high-resolution lake records are being extended further back into the LGM this advancement has exciting implications for volcanic hazard assessment (Fontijn et al., 2014). Very detailed eruptive records are being recognised from within small, closed lake basins and bogs where multiple radiocarbon dates are obtained and robust age models established. Even in upwind localities (e.g. Lago Pichilafquén located near Entre Lagos and upwind (west) from the Puyehue-Antillanca Volcanic Complex) there is an impressive array of eruptives represented that have been effectively under-utilised for volcanic hazard assessment (e.g. Jara and Moreno, 2012). Certainly, sedimentary records from the large lakes in the Chilean Lake District formerly occupied by piedmont glaciers are not as favoured as high-resolution repositories of eruptive and paleoclimate records on account of their lake level histories, multiple inflow sources and potential for sediment redeposition (Bertrand et al., 2014). These lakes are also susceptible to seismically induced subaqueous landsliding events (i.e. Moernaut et al., 2014), which will also adversely influence the overall quality of these records. Lago Teo near Chaitén township (Moreno et al., 2015b) has provided an excellent example of the utility of small and restricted lake/bog basins by indicating a detailed multiple-sourced eruptive record extending over the last 11,000 cal a BP and in addition to its paleoclimate proxy records. In any situation, there are of course caveats: the Lago Teo record cannot be easily reconciled with the record from the equivalent-aged andic soil-forming environment (Moreno et al., 2015b) with some units present in the lake sediments that cannot be correlated to adjacent soil sequences (i.e. LTT-12). However, these issues will likely be clarified in time now that the Lago Teo record is being supported by an array of newly acquired sediment cores from Lago Pinto and Lago Espejo in the vicinity of Futalefú ~72 km to the south-east as well as from lake cores recently retrieved from the vicinity of La Junta located ~128 km to the south-east. Together these records will provide a spatially spread and equivalent-aged data-set by which paleoclimate records in conjunction with eruptive records can be systematically interrogated and assessed.

In Chaitén sector, fine-textured allophane-dominated material intervening between coarser-grained tephra layers varies in chroma intensity (reddish-brown) and degree of soil structure (in this case, blockiness). Taken together these pedogenic features suggest that the intensity of pedogenesis (driven dominantly by variations in temperature and precipitation in combination with vegetation type) affecting tephra deposited at the accreting (upbuilding) paleo-ground surface has varied with time. Such observations are in accord with those documented from an equivalent Southern Hemisphere mid-latitude andic environment from Taranaki, New Zealand, where physical and chemical variations of andic soil successions can be directly linked to prevailing climate (and vegetation) conditions at the time of tephra accretion to the ground surface and its subsequent rapid weathering (see Alloway et al., 1992b,c). Since VCha-sourced tephra are located within specific weathered intervals of the soil succession, they can also be correlated to, and reconciled against, lake sediments where high-resolution palaeo-vegetation trends provide proxy evidence for variations of precipitation, windiness, and fire incidence (natural and/or anthropogenic) (e.g. Henríquez et al., 2015).

The high resolution record from Lago Lepué, located in central-east Isla Grande de Chiloé (43°S), extends continuously from present-day to the end of the LGM (Pesce and Moreno, 2014). Hydroclimate changes in this record, allow reconstruction of past southern westerly wind (SWW) behavior through lake-level variations, past vegetation changes and paleofires. These data indicate lower lake levels and enhanced fire activity between 800 and 2000, 4000–4300, 8000-11,000 and 16,100–17,800 cal a BP, implying reduced SWW influence at 43°S. These intervals alternated with cold, humid phases and muted fire activity (Fig. 19). Comparison of the La Zeta record (see Fig. 8) with sites located near the Pacific coast at the same latitude reveal a stark contrast in terrestrial vegetation, western sites showing an abrupt increase in trees that led to closed-canopy rainforests by 16,000 cal a BP during a warming phase. High abundance in the littoral macrophyte *Isoetes* over this interval suggests shallow lake levels in the Lago Lepué

record (Fig. 19; Pesce and Moreno, 2014). A close examination of the latter reveals the onset of a decline at *c.* 16,800 cal a BP raising the possibility that the La Zeta and Lago Lepué sites record a simultaneous increase in precipitation of westerly origin, considering the confidence intervals of the age models. Can the distribution and depositional character of VCha-sourced tephra be somehow influenced by prevailing climatic conditions across the Andes at the time of eruption?

Already in the soil-forming environment, some interesting occurrences and depositional features might be explained by prevailing climatic conditions at the time of eruption. For instance, the north-westward directed tephra (i.e. Lepué Tephra at *c.* 11,000 cal a BP and Puma Verde Tephra at *c.* 8000 cal. a BP) might relate to a weakened phase of SWW flow interpreted from proxy records between *c.* 7500 and *c.* 11,500 cal a BP. In contrast, the formation of prominent aeolian dune sets in eastern Andean sites (La Zeta) comprising coarse-grained pumiceous ashy constituents of dominantly Pumalín Tephra (LAZ-DII) and an underlying rhyolite of unknown origin (i.e. LAZ-DI) appear to coincide with an episode of strengthening SWW between *c.* 7500 and *c.* 4300 cal. a BP (Fig. 19). Clearly, much more investigation needs to be conducted in order to better establish the connection between volcanic events and climatic conditions that may have influenced tephra distribution, and their occurrence and presentation within the landscape.

6. Conclusion

Our research is intended to provide a comprehensive stratigraphic framework of VCha-sourced tephra for future volcanological and hazard assessment studies. We have also attempted to temporally locate VCha-sourced tephra within a broad paleoenvironmental context so the utility of these tephra can be more widely applied to future inter-regional vegetation/climate and geomorphic studies.

Despite field limitations (e.g. see Section 1.5), a multi-sector proximal to distal inventory of VCha-sourced tephra is presented here with up to 20 discrete rhyolitic events so far identified extending back 18,000 cal a BP (Fig. 19), with at least 10 having widespread areal distributions and/or depositional imprints broadly comparable to, or greater than, the 2008-tephra event. These widespread VCha-sourced tephra are deposited together with tephra from Volcán Michimahuida and many other tephra derived from yet-to-be-resolved eruptive centres and/or point sources. Our results are at odds with the suggestion (e.g. Watt et al., 2013a; Rawson et al., 2016) that the magnitude and/or frequency of volcanism experienced at some Andean volcanic centres may have increased during late last glacial to Holocene times as a result of rapid deglaciation and a corresponding reduction of crustal loading (and hence easing of confining pressures facilitating the upward passage of magma bodies). Many causative factors are at play of which deglaciation is but one. However, for the VCha sector we suggest that in the absence of any LGM-tephra records (whose poor preservation can be directly attributed to widespread Andean piedmont glaciation) creates a significant temporal bias when considering this deglaciation/eruptive magnitude/frequency feedback mechanism. Furthermore, we consider that the relationship between eruptive activity and climate variability over late last glacial to Holocene interval (where excellent records are emerging in both the andic soil-forming, lake/bog and marine environments) should first be scrutinised in detail before any extrapolation back to the LGM.

Our tephrostratigraphic framework indicates that VCha is one of the most continuously active rhyolitic centres in the central and southern portions of the Andean Southern Volcanic Zone (~38°S-46°S) with major- and trace-element glass shard data indicating two closely related magma types and an intermediary 'mixed' type over the last 18,000 years. While the composition of VCha magmas are broadly homogenous over its known history, a newly recognised trachyte-dacite dome of interpreted late Holocene age is identified less than 2-km south-west of VCha. Certainly, one complexity that is immediately apparent in this sector is the eruptive diversity which produce a range of spatially clustered compositions over time from satellite centres within, or adjacent to, the volcanic centre itself (i.e. rhyolite to trachyte dacite to basaltic andesite-basalt, Michimahuida Volcanic Centre) or alternatively within a single eruption (e.g. rhyolite to basalt-andesite, Lepué Tephra sourced from Volcán Michimahuida; see Alloway et al., 2017). As more Andean volcanic centres are being intensively investigated (e.g. Puyehue-Cordón Caulle (Singer et al., 2008; Alloway et al., 2015; Naranjo et al., 2017); Laguna del Maule; (Hildreth et al., 2010; Singer et al., 2014); Volcán Mocho-Choshuenco (Rawson et al., 2015)) this spatially clustered compositional diversity seems to be a more typical feature of the middle and southern sections of the Andes and certainly makes for the prediction of the eruptive type (effusive-explosive, basaltic-rhyolitic), its potential magnitude and impact of future events even more difficult to ascertain with any certainty.

In summary, our studies indicate that eruptive activity centred at VCha has been intermittently continuous for the last 18,000 years. The only opportunity of perhaps retrieving even earlier eruptive records for VCha will likely come from the detailed study of intra-caldera volcaniclastic successions and/or equivalent-aged distal tephra found within high-resolution lake records retrieved from regions located well downwind (east) from VCha and beyond the overwhelming influence of Andean piedmont glaciation. The recognition and correlation of a now extended number of chemically recognisable and chronologically distinguishable VCha-sourced tephra since the LGM associated with other tephra beds from Volcán Michimahuida and other yet-to-be determined eruptive sources from both the soil-forming and lake environments on either side of Andes (western Andean hyper-humid rainforest environment versus eastern Andean semi-arid steppe environment) provides a very tantalising prospect for ongoing and future paleoenvironmental and hazard assessment research advancement.

Acknowledgements

This study was funded by Iniciativa Científica Milenio grants P02-51 and NC120066, Fondecyt 1151469 (to PIM), part funded by a Victoria University of Wellington Science Faculty Research Grant (to BVA), Aberystwyth University Research Fund (to NJGP) and PIP CONICET 2011 0311 (to GV). We thank Craig Wickham, Maria Noel Serra, Lizette Bertin and Jorge Correa for field assistance. We extend our thanks to Ian Schipper for conducting EMP analyses on banded lava float samples from the subsidiary VCha dome. We extend our sincere appreciation to Horacio Griffero and Gabriela Piezug of Posada Kahuel (km-4 Camino Chaitén-Santa Bárbara; www.posadakahuel.cl) for their continuing hospitality and friendship while engaging in field-work. Many thanks to Nicolas La Penna (Chaitur Excursions; www.chaitur.com) for his enthusiastic support and sharing his local knowledge (and fine music talent). We extend our gratitude to the residents of Chaitén township for their hospitality, as well as unwavering willingness, curiosity and support of this research. Finally, we thank Mr Nelson Coombs of Puerto Montt, for expertly flying us over the new Chaitén satellite dome in his immaculate 1966 Piper Cherokee. Finally, the authors would like to acknowledge the two reviewers, David J. Lowe and Karen Fontijn, for their constructive and helpful reviews of this manuscript.

Appendix A. Supplementary data

Supplementary data related to this article can be found at http://dx.doi.org/10.1016/j.quascirev.2017.05.011.

References

Alfano, F., Bonadonna, C., Volentik, A.C.M., Connor, C.B., Watt, S.F.L., Pyle, D.M., Connor, L.J., 2011. Tephra stratigraphy and eruptive volume of the May, 2008, Chaitén eruption, Chile. Bull. Volcanol. 73, 613–630.

Alfano, F., Bonadonna, C., Watt, S., Connor, C., Volentik, A., Pyle, D.M., 2016. Reconstruction of total grain size distribution of the climactic phase of a long-lasting eruption: the example of the 2008-2013 Chaitén eruption. Bull. Volcanol. 78, 46,. http://dx.doi.org/10.1007/s00445-016-1040-5.

Alloway, B.V., Neall, V.E., Vucetich, C.G., 1992a. Particle size analyses of late Quaternary allophane-dominated andesitic deposits from New Zealand. Quat. Int. 13/14, 167–174.

Alloway, B.V., McGlone, M.S., Neall, V.E., Vucetich, C.G., 1992b. The role of Egmont-sourced tephra in evaluating the paleoclimatic correspondence between the bio- and soil-stratigraphic records of central Taranaki. Quat. Int. 13/14, 187–194.

Alloway, B.V., Stewart, R.B., Neall, V.E., Vucetich, C.G., 1992c. Climate of the Last Glaciation in New Zealand, based on aerosolic quartz influx in an andesitic terrain. Quat. Res. 38, 170–179.

Alloway, B.V., Neall, V.E., Vucetich, C.G., 1995. Late Quaternary tephrostratigraphy of northeast and central Taranaki, New Zealand. J. R. Soc. N. Z. 25, 385–458.

Alloway, B.V., Pearce, N.J., Villarosa, G., Outes, V., Moreno, P.I., 2015. Multiple melt bodies fed the AD 2011 eruption of Puyehue-Cordón Caulle, Chile. Nat. Sr. 5, 17589. http://dx.doi.org/10.1038/srep17589.

Alloway, B.V., Moreno, P.I., Pearce, N.J.G., De Pol-Holz, R., Henríquez, W.I., Pesce, O.H., Sagredo, E., Villarosa, G., Outes, V., 2017. Stratigraphy, age and correlation of Lepué Tephra: a widespread *c.*11 cal. ka marker horizon sourced from the Chaitén Sector of southern Chile. J. Quat. Sci. (submitted).

Amigo, A., Lara, L.E., Smith, V.C., 2013. Holocene record of large explosive eruptions from Chaitén and Michimahuida Volcanoes, Chile. Andean Geol. 40, 227–248. http://dx.doi.org/10.5027/andgeoV40n2-a03.

Bertrand, S., Daga, R., Bedert, R., Fontijn, K., 2014. Deposition of the 2011-2012 Cordon Caulle tephra (Chile, 40°S) in lake sediments: implications for tephrochronology and Volcanology. J. Geophys. Res. Earth Surf 119, 2555–2573.

Castro, J.M., Dingwell, D.B., 2009. Rapid ascent of rhyolitic magma at Chaitén Volcano, Chile. Nature 461, 780–783. http://dx.doi.org/10.1038/nature08458.

Denton, G.H., Lowell, T.V., Heusser, C.J., Schlüchter, C., Anderson, B.G., Heusser, L.E., Moreno, P.I., Marchant, D.R., 1999. Geomorphology, stratigraphy and radiocarbon chronology of Llanquihue drift in the area of the Southern Lake District, Seno Relongcaví and Isla Grande de Chiloé, Chile. Geogr. Ann. Ser. A Phys. Geogr. 81B, 167–229.

Fontijn, K., Lachowycz, S.M., Rawson, H., Pyle, D.M., Mather, T.A., Naranjo, J.A., Moreno-Roa, H., 2014. Late Quaternary tephrostratigraphy of southern Chile and Argentina. Quat. Sci. Rev. 89, 70–84.

Fontijn, K., Rawson, H., Van Daele, M., Moernaut, J., Abarzúa, A.M., Heirman, K., Bertrand, S., Pyle, D.M., Matherm, T.A., De Batist, M., Naranjo, J.-A., Moreno, H., 2016. Synchronisation of sedimentary records using tephra: a postglacial tephrochronological model for the Chilean Lake District. Quat. Sci. Rev. 137, 234–254.

Gonzalorena Vallejos, L.A., 2014. Historia postglacial de la vegetación de Lago Tarumán en la zona centro-occidental de Isla Grande de Chiloé: Inferencias paleoambientales a partir de un registro palinológico de alta resolución. Universidad de Chile, Tesis, Magíster en Ciencias Biológicas, Facultad De Ciencias, 84 pp.

Henríquez, W.I., Moreno, P.I., Alloway, B.V., Villarosa, G., 2015. Vegetation and climate change, fire-regime shifts and Volcanic disturbance in Chiloé Continental (43°S) during the last 10,000 years. Quat. Sci. Rev. 123, 158–167.

Hildreth, W., Godoy, E., Fierstein, J., Singer, B.S., 2010. Laguna del Maule Volcanic Field: eruptive history of a Quaternary basalt-rhyolite distributed vent Volcanic fieldon the Andean rangecrest in Central Chile. Serv. Nac. Geol. Mineria, Bol. 63, 145 pp. Santiago, Chile.

Iglesias, V., Whitlock, C., Bianchi, M.M., Villarosa, G., Outes, V., 2012. Holocene climate variability and environmental history at the Patagonian forest/steppe ecotone: Lago Mosquito (42°29'37.89'S, 71°24'14.57'W) and Laguna del Cóndor (42°20'47.22'S, 71°17'07.62'W). Holocene 22, 1297–1307.

Jara, I.A., Moreno, P.I., 2012. Temperate rainforest response to climate change and disturbance agents in northwestern Patagonia (41°S) over the last 2600 years. Quat. Res. 77, 235–244.

Lara, L.E., 2009. The 2008 eruption of the Chaitén Volcano, Chile: a preliminary report. Andean Geol. 36, 125–129.

Lara, L.E., Moreno, R., Amigo, A., Hoblitt, R.P., Pierson, T.C., 2013. Late Holocene history of Chaitén volcano: new evidence for a 17th century eruption. Andean Geol. 40, 249–261. http://dx.doi.org/10.5027/andgeoV40n2-a04.

Lowe, D.J., Tonkin, P.J., 2010. Unravelling Upbuilding Pedogenesis in Tephra and Loess Sequences in New Zealand Using Tephrochronology. Proceedings, IUSS 19th World Congress of Soil Science, Brisbane. Proc. IUSS World Soil Congress Symposium 1.3.2 Geochronological Techniques and Soil Formation, Brisbane, pp. 34–37. August 1-6, 2010. Published on DVD and at. http://www.iuss.org.

Lowe, D.J., Alloway, B.V., 2015. Tephrochronology. In: Rink, W.J., Thompson, J. (Eds.), Encyclopedia of Scientific Dating Methods. Springer, Netherlands, pp. 783–793.

McDaniel, P.A., Lowe, D.J., Arnalds, O., Ping, C.-L., 2012. Andisols. In: Huang, P.M., Li, Y., Sumner, M.E. (Eds.), Handbook of Soil Sciences, second ed., vol. 1. Properties and Processes. CRC Press (Taylor & Francis), Boca Raton, Florida, pp. 33.29–33.48.

Martin, R.S., Watt, S.F.L., Pyle, D.M., Mather, T.A., Matthews, N.E., Georg, R.B., Day, J.A., Fairhead, T., Witt, M.L.I., Quayle, B.M., 2009. Environmental effects of ashfall in Argentina from the 2008 Chaitén Volcanic eruption. J. Volcanol. Geotherm. Res. 184, 462–472.

Moernaut, J., Van Daele, M., Heirman, K., Fontijn, K., Strasser, M., Pino, M., Urrutia, R., De Batist, M., 2014. Lacustrine turbidites as a tool for quantitative earthquake reconstruction: new evidence for a variable rupture mode in south-central Chile. J. Geophys. Res. Solid Earth 119, 1607–1633.

Moreno, P.I., Denton, G.H., Moreno, H., Lowell, T.V., Putnam, A.E., Kaplan, M.R., 2015a. Radiocarbon chronology of the last glacial maximum and its termination in northwestern Patagonia. Quat. Sci. Rev. 122, 233–249.

Moreno, P.I., Alloway, B.V., Henriquez, W.I., Villarosa, G., Outes, V., De Pol-Holz, R., Pearce, N.J.G., 2015b. A past millennium maximum in postglacial activity from Volcán Chaitén, southern Chile. Geology 43, 47–50.

Murphy, M.A., Salvador, A. (Eds.), 1999. International Stratigraphic Guide - an Abridged Edition. Episodes, vol. 22, pp. 255–271.

Naranjo, J.A., Stern, C.R., 2004. Holocene tephrochronology of the southernmost part (42°30'- 45°S) of the andean Southern volcanic Zone. Rev. Geol. Chile 31, 225–240.

Naranjo, J.A., Singer, B.S., Jicha, B.R., Moreno, H., Lara, L.E., 2017. Holocene tephra succession of Puyehue-Cordón Caulle and Antillanca/Casablanca volcanic complexes, southern Andes (40-41°S). J. Volcanol. Geotherm. Res. http://dx.doi.org/10.1016/j.jvolgeores.2016.11.017.

Osores, M.S., Folch, A., Collini, E., Villarosa, G., Durant, A., Pujol, G., Viramonte, J.G., 2013. Validation of the FALL3D model for the 2008 Chaitén eruption using field and satellite data. Andean Geol. 40, 262–276.

Parfitt, R.L., Clayden, B., 1991. Andisols – the development of a new order in Soil Taxonomy. Geoderma 49, 181–198.

Pesce, O.H., Moreno, P.I., 2014. Vegetation, fire and climate change in central-east Isla Grande de Chiloé (43°S) since the Last Glacial Maximum, northwestern Patagonia. Quat. Sci. Rev. 90, 143–157.

Rawson, H., Naranjo, J.-A., Smith, V., Fontijn, K., Pyle, D.M., Mather, T.A., Moreno, H., 2015. The frequency and magnitude of post-glacial explosive eruptions at Volcán Mocho-Choshuenco, southern Chile. J. Volcanol. Geotherm. Res. 299, 103–129.

Rawson, H., Pyle, D.M., Mather, T.A., Smith, V.C., Fontijn, K., Lachowycz, S.M., Naranjo, J.A., 2016. The magmatic and eruptive response of arc Volcanoes to deglaciation: insights from southern Chile. Geology 44 (4), 251–254. http://dx.doi.org/10.1130/G37504.1.

Shane, P.A., Martin, S.B., Smith, V.C., Beggs, K.F., Darragh, M.B., Cole, J.W., Nairn, I.A., 2007. Multiple rhyolitic magmas and basalt injection in the 17.7 ka Rerewhakaaitu eruption episode from Tarawera volcanic complex, New Zealand. J. Volcanol. Geotherm. Res. 164, 1–26.

Singer, B.S., Jicha, B.R., Harper, M.A., Naranjo, J.A., Lara, L.E., Moreno-Roa, H., 2008. Eruptive history, geochronology, and magmatic evolution of the Puyehue-Cordón Caulle Volcanic complex, Chile. Geol. Soc. Am. Bull. 120, 599–618.

Singer, B.S., Anderson, N.L., Le Mével, H., Feigl, K.L., DeMets, C., Tikoff, B., Thurber, C.H., Cardona, C., Córdova, L., Gil, F., Unsworth, M.J., Williams-Jones, G., Miller, C., Fierstein, J., Hildreth, W., Vazquez, J., 2014. Dynamics of a large, restless, rhyolitic magma system at Laguna del Maule, southern Andes, Chile. GSA Today 24, 4–10.

Smith, G.D., 1984. The andic soil proposal 1978: a preliminary proposal for reclassification of andepts and andic soil sub-groups. N. Z. Soil Bur. Rec. 96.

Soil Survey Staff, 2014. Keys to Soil Taxonomy, twelfth ed. USDA-Natural Resources Conservation Service, Washington, DC, p. 360.

Watt, S.F.L., Pyle, D.M., Mather, T.A., Martin, R.S., Matthews, N.E., 2009. Fallout and distribution of volcanic ash over Argentina following the May 2008 explosive eruption of Chaitén, Chile. J. Geophys. Res. 114, B04207. http://dx.doi.org/10.1029/2008JB006219.

Watt, S.F.L., Pyle, D.M., Naranjo, J.-A., Rosqvist, G., Mella, M., Mather, T.A., Moreno, H., 2011. Holocene tephrochronology of the Hualaihue region (Andean southern Volcanic zone, ~42°S), southern Chile. Quat. Int. 246, 324–343.

Watt, S.F.L., Pyle, D.M., Mather, T.A., 2013a. The Volcanic response to deglaciation: evidence from glaciated arcs and a reassessment of global eruption records. Earth Sci. Rev. 122, 77–102.

Watt, S.F.L., Pyle, D.M., Mather, T.A., 2013b. Evidence of mid- to late-Holocene explosive rhyolitic eruptions from Chaitén Volcano, Chile. Andean Geol. 40, 216–226. http://dx.doi.org/10.5027/andgeoV40n2-a02.

Watt, S.F.L., Gilbert, J.S., Folch, A., Phillips, J.C., Cai, X.M., 2015. An example of enhanced tephra deposition driven by topographically induced atmospheric turbulence. Bull. Volcanol. 77, 1–14.

Wicks, C., de la Llera, J.C., Lara, L.E., Lowenstern, J., 2011. The role of dyking and fault control in the rapid onset of eruption at Chaitén Volcano. Chile Nat. 478, 374. http://dx.doi.org/10.1038/nature10541.